nature biomedical engineering

Article

https://doi.org/10.1038/s41551-025-01380-1

Sensitization of tumours to immunotherapy by boosting early type-I interferon responses enables epitope spreading

Received: 17 August 2023

Accepted: 24 March 2025

Published online: 18 July 2025

Check for updates

Sadeem Qdaisat[1,2,11], Brandon Wummer[1,11], Brian D. Stover[3,11], Dingpeng Zhang[1], James McGuiness[1], Frances Weidert[1], Jonathan Chardon-Robles[1], Adam Grippin[4], Anna DeVries[1], Chong Zhao[1], Christiano Marconi[1], Aida Karachi[1], Chao Xie[1], Gabriel Jobin[3], Ruixuan Liu[1], Stephen Michel[1], Xiaojie Ma[3], Rachel S. F. Moor[1], Christina von Roemeling[1], Duy T. Nguyen[5], Leighton Elliott[6], Nagheme Thomas[1], Arnav Barpujari[3], Hilary Geffrard[1], Yodarlynis Campaneria[1], Elizabeth Ogando-Rivas[1], Cathleen Rabideau[3], Dhruvkumar Soni[1], Jianping Huang[1], Sheila Carrera-Justiz[7], Kristianna Fredenburg[8], Natalie L. Silver[9], W. Gregory Sawyer[5], Maryam Rahman[1], John A. Ligon[3], Catherine T. Flores[1], Ji-Hyun Lee[10], Duane A. Mitchell[1], Paul Castillo[3], Hector R. Mendez-Gomez[1] & Elias J. Sayour[1,3] ✉

The success of cancer immunotherapies is predicated on the targeting of highly expressed neoepitopes, which preferentially favours malignancies with high mutational burden. Here we show that early responses by type-I interferons mediate the success of immune checkpoint inhibitors as well as epitope spreading in poorly immunogenic tumours and that these interferon responses can be enhanced via systemic administration of lipid particles loaded with RNA coding for tumour-unspecific antigens. In mice, the immune responses of tumours sensitive to checkpoint inhibitors were transferable to resistant tumours and resulted in heightened immunity with antigenic spreading that protected the animals from tumour rechallenge. Our findings show that the resistance of tumours to immunotherapy is dictated by the absence of a damage response, which can be restored by boosting early type-I interferon responses to enable epitope spreading and self-amplifying responses in treatment-refractory tumours.

Immune checkpoint inhibitors (ICIs) have revolutionized cancer therapy[1,2]. By blocking the pathways that regulate the immune system, these monoclonal antibodies (mAb) can enhance immunity, boost T-cell activity and reinitiate the recognition and destruction of cancer cells[3–6]. Successful ICI therapy is predicated on an activated T-cell response against cancer neoepitopes which preferentially favours malignancies with high tumour mutational burdens (TMB)[7–9]. However, many TMB-high tumours are ICI resistant and TMB-low cancers may have limited cases of patient responders[10–12]. The interplay driving cancer immunogenicity and response to immunotherapy remains poorly understood.

Interferon (IFN) signalling has been implicated as an important mechanism in both resistance and therapeutic susceptibility[13]. In established tumours, IFN production instigates both epigenomic and transcriptomic modifications that foster tumour resistance[14]. Many tumours manage to develop ICI resistance by hijacking type-I IFN

A full list of affiliations appears at the end of the paper. ✉e-mail: Elias.Sayour@neurosurgery.ufl.edu

https://doi.org/10.1038/s41551-025-01380-1

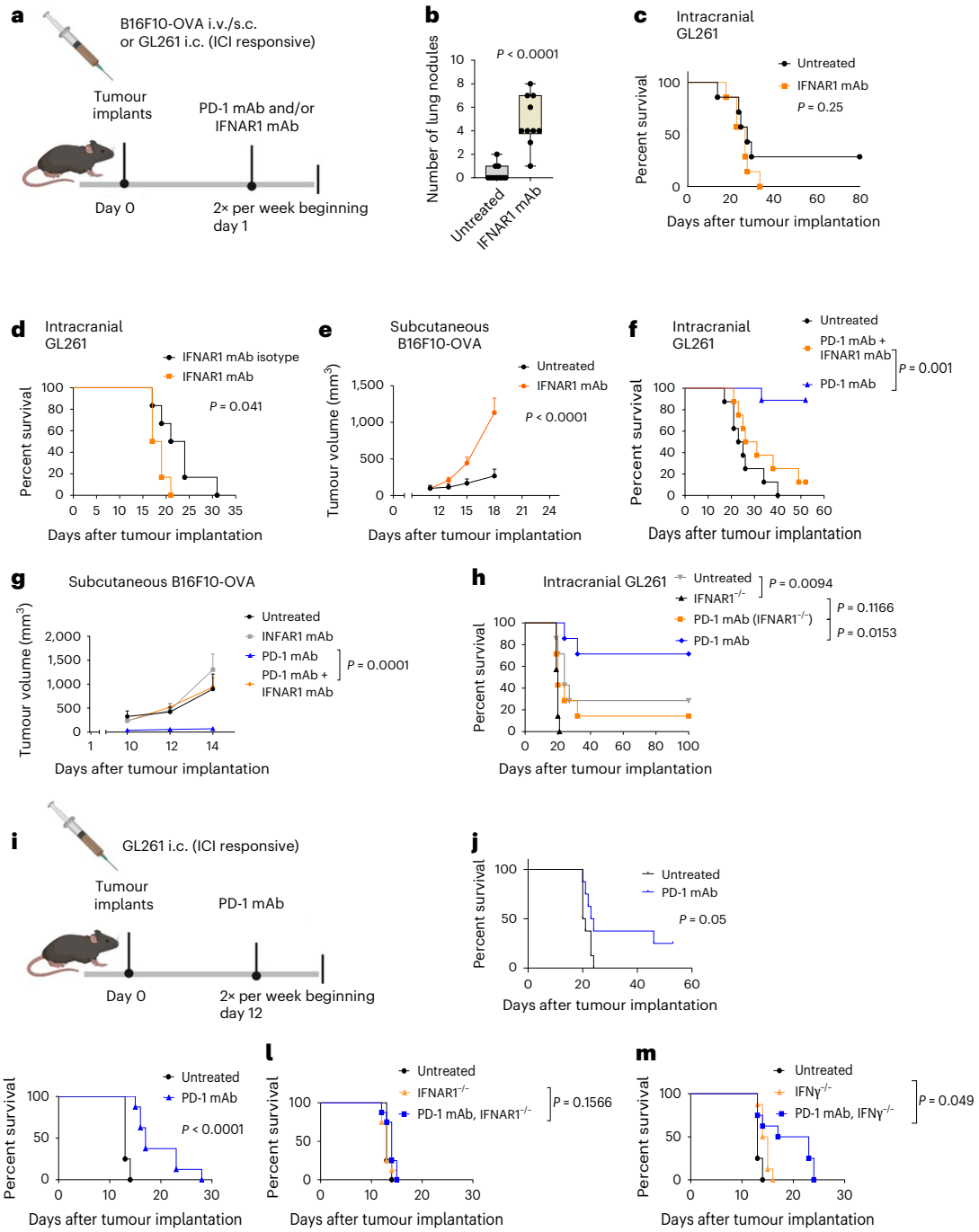

Fig. 1 | IFN-I is necessary for complete tumourigenicity and response to ICIs. **a**, Treatment schema. **b**, Boxplot of B16F10-OVA melanoma injected into either untreated C57Bl/6 mice or mice treated with IFNAR1 mAb; $n = 10$ per group. IFNAR1 mAbs were administered as a loading dose before and after tumour implantation, and maintenance dosing was continued twice weekly. Lungs were collected on day 14 and tumour nodules per lung were enumerated. **c**, Kaplan–Meier survival curve of C57Bl/6 mice ($n = 7$ per group) implanted intracranially (i.c.) with non-tumourigenic GL261 glioma cells, treated with intraperitoneal (i.p.) IFNAR1 mAb compared to untreated animals. **d**, Kaplan–Meier survival curve of C57Bl/6 mice ($n = 6$ per group) implanted i.c. with tumourigenic GL261 glioma cells, treated with i.p. IFNAR1 mAb compared with animals receiving IFNAR1 isotype mAbs. **e**, Tumour volume growth curve of B16F10-OVA tumours in C57Bl/6 mice ($n = 7$ per group) implanted subcutaneously (s.c.) with B16F0 and B16F10-OVA melanoma cells in contralateral flanks before i.p. treatment with IFNAR1 mAb. **f**, Kaplan–Meier survival curve of C57Bl/6 mice ($n = 8$–9 per group) implanted i.c. with GL261 glioma cells and treated with PD-1 mAb alone or in combination with IFNAR1 mAb. **g**, Tumour growth curve of C57Bl/6 mice ($n = 8$ per group) implanted subcutaneously with B16F10-OVA melanomas, treated with PD-1 mAb, IFNAR1 mAb or PD-1 + IFNAR1 mAb. **h**, Kaplan–Meier survival curve of both wild-type C57Bl/6 and IFNAR1 KO mice ($n = 7$ per group) i.c. implanted with GL261 glioma cells and treated with PD-1 mAb compared with untreated control groups. **i**, Treatment schema for **j**–**m**. **j**, Kaplan–Meier survival curve of C57Bl/6 mice ($n = 8$ per group) implanted i.c. with GL261 glioma cells and treated with PD-1 mAb. **k**–**m**, Kaplan–Meier survival curve of C57Bl/6 mice ($n = 8$ per group) implanted i.c. with GL261 undergoing treatment with PD-1 mAb in wild-type animals (**k**), IFNAR1 knockout mice (**l**) and IFNγ knockout mice (**m**). Significance was determined using Mann–Whitney test (**b**), log-rank test (**c**,**d**,**f**,**h**,**j**–**m**) and mixed-effect analysis/two-way ANOVA (**e**,**g**). Boxplots display box at first and third quartile with line at median and whiskers from minimum to maximum datapoint values (**b**). Error bars are reported as s.e.m. (**e**,**g**). Panels **a** and **i** created with BioRender.com.

(IFN-I) signalling pathways, thus thwarting the induction of therapeutic immunity[15]. Sustained IFN-I production can precipitate an immunoregulatory state and a chronic inflammatory milieu deleterious to adaptive immunity and response to ICIs[16,17].

However, IFN-I is vital for immunologic response through pattern recognition receptor activation and plays a vital role in facilitating interactions between dendritic cells and effector T cells[18,19]. On the basis of these effects, we hypothesized that early IFN-I is critical for initiating cancer immunotherapy and epitope spreading in immunogenic malignancies, and could be artificially induced by RNA-encoding biomimetics in poorly immunogenic tumours. We found that early IFN-I shaped the magnitude of ICI response in both intra and extracranial murine solid tumours and dictated cancer immunogenicity in ICI-responsive tumours in a manner that was transferable to previously resistant malignancies. We leveraged this understanding towards the development of non-tumour-specific messenger RNA vaccines that restored IFN-I-dependent immunity in parallel models for ICI-resistant tumours, enabling epitope spreading and improved survivorship.

Results

We investigated IFN-I effects on tumourigenesis in strongly immunogenic malignancies such as B16F10-OVA, injected intravenously (i.v.) to simulate metastatic tumour seeding (Fig. 1a). We found that administration of IFN-I receptor blocking mAb (IFNAR1 mAb) facilitated uniform tumour development following 150,000 cells, a tumour cell dose that typically produces tumours in only 25% of untreated mice (Supplementary Fig. 1). Mice treated with IFNAR1 mAb developed more lung nodules than untreated mice (Fig. 1b), suggesting that early IFN-I signalling facilitates immune surveillance and regulation of tumour growth, while its absence can lead to complete tumourigenesis. To uncover whether these observations might apply to intracranial tumours, we selected an immunogenic intracranial glioma model (GL261, using a non-tumourigenic dose) where simultaneous blockade of IFN-I signalling promoted complete tumourigenesis (Fig. 1c). When repeated with completely tumourigenic doses of GL261 or B16F10-OVA, animals receiving IFNAR1 mAbs had more aggressive tumours than control mice (Fig. 1d,e). We then conducted a series of experiments assessing the effects of IFN-I on ICI sensitivity in prototypically responsive GL261 and B16F10-OVA tumours. After tumour implantation, mice were treated with biweekly PD-1 blockade, with or without IFNAR1 blocking mAbs. Although early administration of PD-1 mAb significantly enhanced survival and suppressed tumour growth, the introduction of IFNAR1 blocking antibodies markedly mitigated survival outcomes (Fig. 1f,g, and Supplementary Figs. 2 and 3). These data highlight the critical role of IFN-I in modulating cancer immunogenicity and response to checkpoint inhibitors in both extracranial and intracranial tumour models.

In repeat experiments with isotype controls (Supplementary Fig. 4), we found that mAb isotype can adversely affect response to PD-1 mAb perhaps through non-specific interaction with PD-1 receptor or through saturation of IgG receptors. To substantiate whether IFNAR1 played a key biological role in the response to PD-1 mAb, we replicated these experiments in IFNAR1 knockout (KO) mice. In IFNAR1 KO animals bearing GL261 tumours, mice did not have significantly improved survivorship following PD-1 mAb therapy, confirming the necessity of IFN-I in eliciting ICI responsiveness (Fig. 1h). While these results demonstrate the importance of innate immunity and IFNAR1 signalling for ICI response, in these experiments ICI treatment was started at early timepoints (days 1–5). To demonstrate that early interferon response could also impact ICI treatment at later timepoints, we treated intracranial GL261-bearing mice with anti-PD-1 mAbs beginning treatment on day 12 (Fig. 1i), which resulted in significant activity (Fig. 1j–m). Interestingly, in these late-treatment models, there were no significant differences between untreated mice and IFNAR1 knockout animals, suggesting that the endogenous immune response can be overcome by more aggressive tumours. We then sought to assess the impact of type II interferon on ICI response in late-treatment models for GL261. Unlike the blockade of IFN-I receptor signalling, which eliminates ICI effectivity, blockade of type II IFN did not abrogate survivorship (Fig. 1k–m).

Since IFN-I plays a pivotal role in the response to PD-1 mAb, we postulated that myeloid cells might be crucial in mediating ICI activity. We sequenced GL261 tumours from untreated and PD-1-treated wild-type, IFNAR1 knockout and IFNγ knockout animals. In untreated animals, there was presence of endogenous immunity with cytotoxic cells, natural killer (NK) cells and macrophages that became attenuated in IFNAR1 and IFNγ knockout mice (Fig. 2a). PD-1 blockade increased gene signatures for NK cells and macrophages in the tumour microenvironment (TME) of IFNγ knockout mice, which perhaps compensated for poorly cytotoxic T cells; however, macrophages remained decreased in IFNAR1 knockout mice, suggesting these cells to be critical for response to anti-PD-1 treatment (Fig. 2b). To further demonstrate the importance of macrophages and myeloid cells in response to ICIs, we showed that non-specific depletion of myeloid cells (phagocytes) with clodronate liposomes (LP) (Fig. 2c) elicits a trend towards decreased long-term survival following PD-1 mAbs (Fig. 2d and Supplementary Fig. 5). Thus, while myeloid cells are a notable immunoregulatory compartment in many malignancies including the glioma microenvironment, their intratumoural presence following IFN-I signalling appears essential for eliciting maximal ICI activity.

Although anti-tumour immunity from ICIs was dependent on IFN-I in the TME, we theorized that this was due to polarization of adaptive immunity from strongly immunogenic driver antigens and sought to assess whether ICI sensitivity was transferrable to resistant models. To model this, mice with ICI-sensitive tumours (B16F10-OVA) were treated with anti-PD-1 mAb in the presence or absence of IFN-I receptor (IFNAR1) inhibition, and following treatment, splenic $CD3^+$ lymphocytes were collected and transferred to a new group of mice with ICI-resistant tumours with shared tumour antigens (B16F0) (Fig. 2e). Our findings revealed that CD3-selected T cells from PD-1-treated B16F10-OVA-bearing mice (CD3splen) were able to initiate a potent anti-tumour response against normally ICI-resistant tumours (B16F0) in recipient mice; however, CD3-selected T cells from donor mice treated with early IFNAR1 mAb imparted no benefit, suggesting that ICI sensitivity is dependent on early IFN-I signalling with the capacity to elicit antigenicity against weaker non-OVA antigens in B16F0-bearing animals (Fig. 2e). These results highlight that the presence of a single strong antigen (that is, OVA) may be sufficient to induce IFN-I response and epitope spread against poorly immunogenic tumour antigens that are transferrable to non-OVA-expressing tumours. To confirm these data, we designed a separate but related experiment where we inoculated the same mouse with both a subcutaneous ICI-sensitive tumour (B16F10-OVA) and an ICI-resistant tumour (B16F0) with shared antigens, followed by treatment with PD-1 mAb with or without IFN-I receptor blockade (Fig. 2f). The presence of B16F10-OVA on the contralateral flank was enough to unlock B16F0's sensitivity to PD-1 mAb, an effect that was abrogated in the presence of early IFN-I receptor inhibition (Fig. 2f).

Since there was no significant change observed in the kinetics of tumour growth following IFNAR1 blockade in B16F0 tumours (Fig. 3a), but instead an IFNAR1-dependent response following transfer of non-specific driver antigens (Fig. 2f), we sought to develop approaches for resetting IFN-I signalling in ICI-resistant tumour models (that is, B16F0). We postulated that introduction of intratumoural IFNα during tumourigenesis was critical for tumour immunogenicity—an effect that could be achieved by simply culturing tumour cells with IFNα before implantation. In the presence (Fig. 3b and Supplementary Fig. 6) or absence of ICI therapy (Fig. 3c), intratumoural IFN-I following co-culture and/or co-administration was sufficient to delay tumour growth. To determine whether these effects were strictly mediated by the innate immune response, we repeated these experiments in SCID mice. Although there was delayed tumour growth in SCID

https://doi.org/10.1038/s41551-025-01380-1

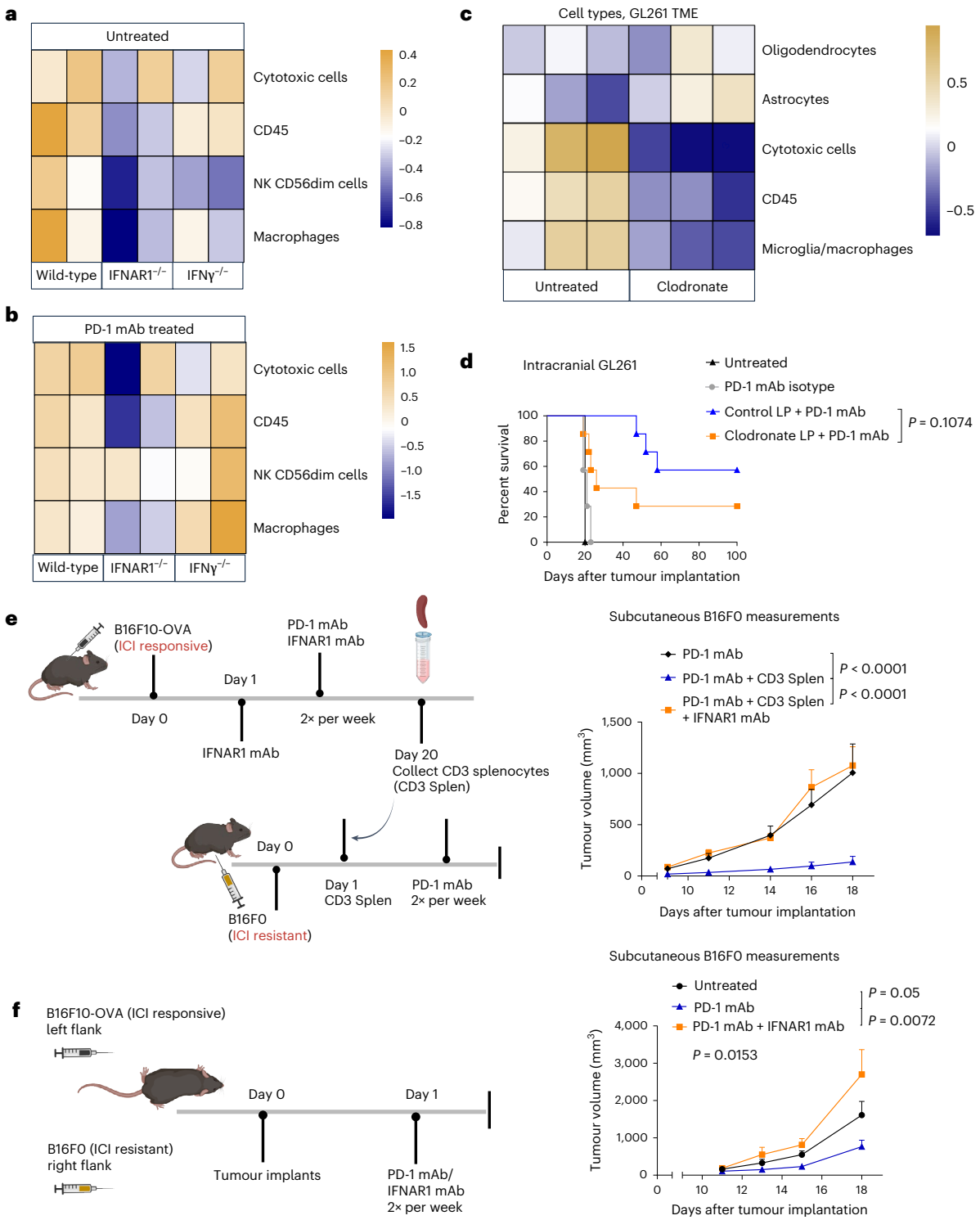

Fig. 2 | Sensitivity to ICIs is transferrable to resistant models in an IFNAR1-dependent manner. a,**b**, Nanostring profiling of GL261 from untreated (**a**) versus late PD-1 (day 12)-treated (**b**) wild-type IFNAR1 and IFNγ knockout mice ($n = 2$ per group). **c**, Brain tumours (GL261) collected from inoculated mice ($n = 3$ per group) were left untreated or treated with clodronate before nanostring analysis of immune cells and microglia. **d**, Kaplan–Meier survival curve for C57Bl/6 mice ($n = 4$–7 per group) implanted intracranially with GL261 glioma cells, treated with clodronate or control liposomes (LP, 200 µl), administered intravenously 24 h before tumour implantation. **e**, Left: experimental diagram of donor mice ($n = 7$ per group) inoculated with B16F10-OVA cells and treated intraperitoneally (i.p.) with biweekly PD-1 mAb alone or in combination with early i.p. IFNAR1 mAb. $CD3^+$ splenocytes (CD3 Splen) were collected from mice 20 days post tumour implantation and transferred to recipient mice inoculated with ICI-resistant B16F0 cells. Right: The recipient mice were then treated with biweekly PD-1 mAb and tumour growth curves were plotted. CD3 Splen, CD3 splenocytes from ICI-sensitive B16F10-OVA. **f**, Left: experimental diagram showing mice ($n = 7$ per group) inoculated with B16F10-OVA and B16F0 implanted into contralateral flanks, treated i.p. with PD-1 mAb with or without IFNAR1 mAb. Right: tumour volume measurements of B16F0 tumours. Statistical significance was determined using log-rank test (**d**) and mixed-effect analysis/two-way ANOVA (**e**,**f**). Colour bars for heat maps represent distribution for cell types by Z-score (**a**–**c**). Error bars are reported as s.e.m. Panels **e** and **f** created with BioRender.com.

mice receiving intratumoural IFN-I, there was enhanced response in wild-type mice receiving both intratumoural IFN-I and anti-PD-1 therapy (Fig. 3d). We surmised that these effects were partially attributable to an increase in major histocompatibility complex (MHC)-I expression and programmed death-ligand 1 (PD-L1) on B16F0 cells which we observed in ex vivo studies following co-culture with IFN-I cytokines (Fig. 3e–g and Supplementary Figs. 7–10). When combined with T cells specific for B16F0 antigens (that is, P-mel), there appeared to be increases in class I/II expression on tumour cells, highlighting the importance of adaptive immunity in amplifying the initial innate response induced by IFN-I (Supplementary Fig. 10). Taken together, these data suggest that early localized IFN-I production at the tumour site is a key driver of ICI sensitivity mediated in part through adaptive mechanisms for antigen recognition.

We sought to develop methods that could sensitize poorly immunogenic tumours by boosting the early IFN-I response in a translational manner. To develop this understanding into a translatable approach, we examined whether RNA-loaded biomimetics encoding for non-tumour-specific IFN-I driver antigens could achieve similar effects to intratumoural inoculation of IFN-I. We leveraged RNA–nanoparticle preparations that would quickly depot in parenchymal organs[20,21]. We also selected a uridine-containing non-tumour-specific mRNA (uRNA; Fig. 4a) on the basis of its ability to elicit superior IFN-I responses over modified (pseudouridine modified, silenced) mRNA (modRNA; Fig. 4b,c) which are utilized in commercial lipid nanoparticle (LNP) preparations. While modRNA have been revolutionary for unlocking the message in mRNA vaccines targeting SARS-CoV-2, as evidenced by the recent Nobel Prize for the pioneering work of Drs Weissman and Kariko[22], we show that uRNA may be superior to modRNA in therapeutic cancer vaccine formulations (Fig. 4d). On the basis of these results, we designed follow-up experiments testing the immunogenicity and efficacy of uRNAs encoding for immunogenic non-tumour-specific proteins in poorly immunogenic murine models (that is, B16F0). It has previously been shown that luciferase-transduced tumours are more immunogenic with increased survival benefits, suggesting luciferase to be a strong IFN-I driver antigen[23]. We tested whether luciferase-encoding uRNA in nanoparticle preparations would sensitize response to ICIs. In a subcutaneous model of B16F0, luciferase-encoding uRNA mediated anti-tumour efficacy with significant synergy in combination with ICIs (Fig. 4e,f). In these tumours, there was concordance with decreasing tumour volume size and increased tumour-infiltrating lymphocytes (TILs) and PD-1$^+$CD8$^+$ cells (Fig. 4g–i and Supplementary Fig. 11). These changes were concordant with changes in the periphery where we observed an increase in PD-1$^+$CD8$^+$ cells in the spleens of treated animals (Fig. 4j).

To follow up on these results and to determine whether RNA vaccines might be effective as monotherapies, we developed optimized formulations composed of multilamellar (ML) uRNA-loaded lipid particle aggregates (uRNA LPAs) using our previously described methods[24]. Following intravenous (i.v.) administration of ML uRNA (Fig. 5a), there was rapid induction of IFN-I (IFNβ) (Fig. 5b) and principal uptake in the lungs of mice (Fig. 5c). On the basis of these findings, we hypothesized that monotherapy with ML uRNA encoding for non-tumour-specific immunogens would be optimal against pulmonary tumours. We tested immunogenic IFN-I driver antigen (that is, GFP) in poorly immunogenic murine models for pulmonary osteosarcoma and melanoma (Fig. 5d)[25]. Compared with untreated or ICI-treated animals, ML uRNA encoding for GFP elicited fewer pulmonary nodules and improved survival outcomes (Fig. 5e–h). ML uRNA activated multiple pattern recognition receptors responsible for induction of IFN-I (Fig. 5i), and IFN-I was requisite for long-term survivorship (Fig. 5j). Despite the significant IFN-I response observed in these animals, we show that ML uRNA was relatively well tolerated in tumour-bearing mice based on stable weights (Fig. 5k). While responses were completely dependent on IFN-I signalling, efficacy was only partly dependent on T-cell immunity (Fig. 5l,m). Interestingly, there was significant worsening of tumour volumes following CD8 blockade, but not following CD4 blockade (Fig. 5m), which could be due to the elimination of both tumour-reactive CD4 cells and regulatory T cells. In animals vaccinated with ML uRNA, there were increases in intratumoural CD45$^+$ cells and T cells including regulatory T-cell populations (Supplementary Fig. 12).

Next, we sought to assess the immunologic phenotype induced by ML uRNA. We show that ML uRNA can induce other pro-inflammatory cytokines, in addition to IFN-I, including Th1 cytokines and T-cell recruiting chemokines which rapidly defervesce by 24 h (Fig. 6a–c). These changes are necessary to recruit T-cell responses to the TME of mice bearing pulmonary tumours, and IFN-I was critical for dictating the magnitude of the chemokine response, as levels of dendritic cell (DC) and T-cell recruiting chemokines (CCL3 and CCL4) were significantly attenuated following IFNAR1 blockade (Fig. 6d). In mice bearing K7M2 pulmonary tumours, we show that repeated treatment with ML uRNA reprograms the TME into a pro-inflammatory milieu with increased central memory T cells (Fig. 6e). In a separate experiment, we profiled the spleen from animals vaccinated with serial ML uRNA and found a significant increase in activated T cells denoted by increased expression of CD69 and 4-1BB on CD4 and CD8 cell subsets (Fig. 6f). These changes demonstrate the ability of ML uRNA to influence evolution of the TME from a myeloid suppressive milieu to a T-cell enabling landscape. We performed nanostring genomic analysis on the TME of animals treated with serial ML uRNA and revealed increased gene signatures for T cells and activation markers, and decreased signatures for genes associated with myeloid-derived suppressor cells (CD14) and tumour-associated macrophages (CD68) (Fig. 6g–m). Increased gene signatures for antigen processing and presentation machinery are suggestive of de novo priming of antigen-reactive T cells (Fig. 6k,l). These findings correlated with increased DCs and cytolytic cells that were attenuated following concomitant treatment with IFNAR1 mAbs (Fig. 6m). Intratumoural changes mediated by ML uRNA were concordant at the beginning and throughout treatment in early- versus late-treatment models (Supplementary Fig. 13). Thus, serial administration of non-tumour-specific antigens can reset the immunologic milieu in favour of effector T cells, which are critical for sustained immunologic response.

Since luciferase and GFP-encoding uRNAs are not readily translatable, we tested whether ML uRNA encoding for an immunogenic human viral protein (CMV matrix protein pp65) would elicit similar effects. In SCID mice intravenously implanted with human cell lines, KHOS and 143B tumour cells to model metastatic pulmonary human osteosarcoma (Fig. 7a), we observed significant improvement in survival benefit following ML uRNA coding for pp65 (Fig. 7b). To ensure that ML uRNA could elicit long-term immunity with memory recall response, we vaccinated immunocompetent Balb/c mice inoculated with pulmonary K7M2 and rechallenged long-term survivors after 100 days (Fig. 7c). We compared different non-tumour-specific ML uRNA formulations encoding for GFP and pp65. Since pp65 is flanked by a full-length lysosomal membrane protein (human LAMP), we rationalized that longer uRNAs might be more immunogenic. In mice bearing pulmonary osteosarcomas from K7M2 inoculation, we observed possible differences in anti-tumour immunity from GFP versus pp65 (Fig. 7d), which might be secondary to the innate immunogenicity of each protein, or due to the longer transcript length of pp65. Upon rechallenge, half of the long-term survivors across both ML uRNA groups (GFP and pp65) were able to successfully ward off tumours (Fig. 7e), suggesting the ability to develop adaptive immunity from epitope spreading. Since vaccines were administered soon after tumour implantation in the previous studies, we wanted to investigate whether ML uRNA could elicit improved survivorship in late-stage tumour models. We chose another paediatric tumour to model late-stage disease as these tend to be immunologically ‘cold’. In neonatal mice bearing midline K2 diffuse midline gliomas (DMG), beginning treatment ~30 days after

https://doi.org/10.1038/s41551-025-01380-1

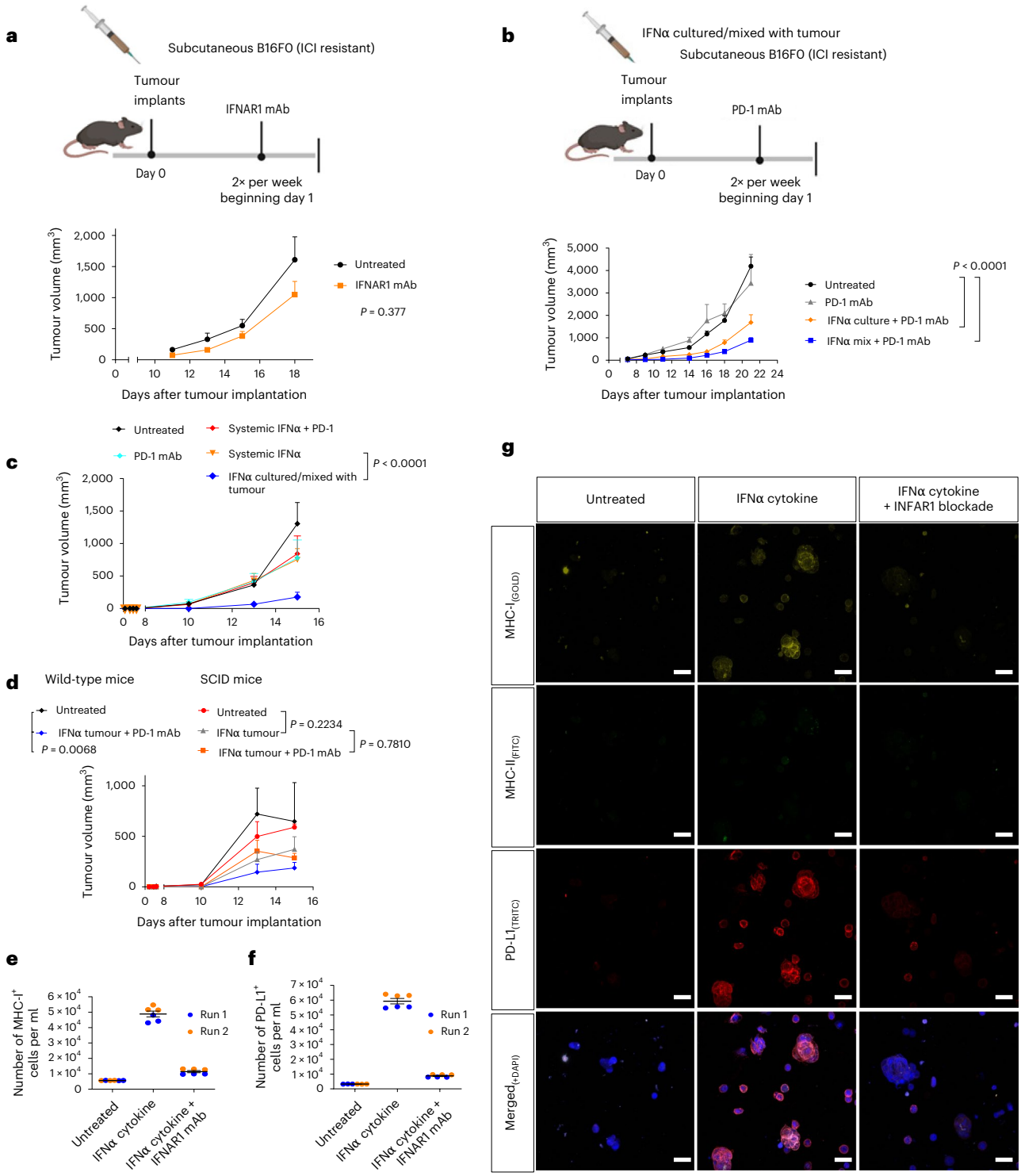

Fig. 3 | Early IFN-I treatment sensitizes antigen recognition and ICI response. **a**, Tumour volume growth curve of B16F10 tumours in C57Bl/6 mice ($n = 7$ per group) implanted subcutaneously with B16F0 and B16F10-OVA melanoma cells in contralateral flanks treated i.p. with IFNAR1 mAb. Untreated mice from Fig. 2f were concurrently measured as a comparator group. **b**, Tumour growth curve from C57Bl/6 mice ($n = 7$ per group) implanted with B16F0 melanomas. IFNα was either directly added in co-culture with B16F0 cells (IFNα culture) or mixed with B16F0 cells (IFNα mix) before tumour implantation, followed by treatment with PD-1 mAbs. **c**, Tumour growth curve for C57Bl/6 mice ($n = 8$ per group) implanted with subcutaneous B16F0 melanomas. IFNα was directly added in co-culture with B16F0 cells, followed by mixture with B16F0 cells before tumour implantation. Animals were compared to mice receiving PD-1 mAb or systemic IFNα alone and in combination. **d**, Tumour volume measurements of wild-type versus SCID mice ($n = 7$–8 per group) implanted with subcutaneous B16F0 melanomas treated with intratumoural IFNα with and without PD-1 mAb. IFNα was directly added in co-culture with B16F0 cells, followed by mixture with B16F0 cells before tumour implantation (IFNα tumour). **e**,**f**, B16F0 melanomas were cultured in vitro with IFNα cytokine or IFNα cytokine + IFNAR1 mAb for 24 h versus an untreated group. Cells were then collected for flow cytometric analysis of MHC-I-positive (**e**) and PD-L1-positive (**f**) cells (2 biological replicates each with 3 technical replicates are shown in different colours). **g**, Immunofluorescence images depicting MHC-I, PD-L1 and MHC-II expression in 3D spheroids of B16F0 melanoma treated with IFNα cytokine with and without IFNAR1 mAbs. Scale bars, 50 µm. Significance was determined using mixed-effect analysis/ANOVA (**a**–**d**). Error bars are reported as s.e.m. (**a**–**f**). Panels **a** and **b** created with BioRender.com.

https://doi.org/10.1038/s41551-025-01380-1

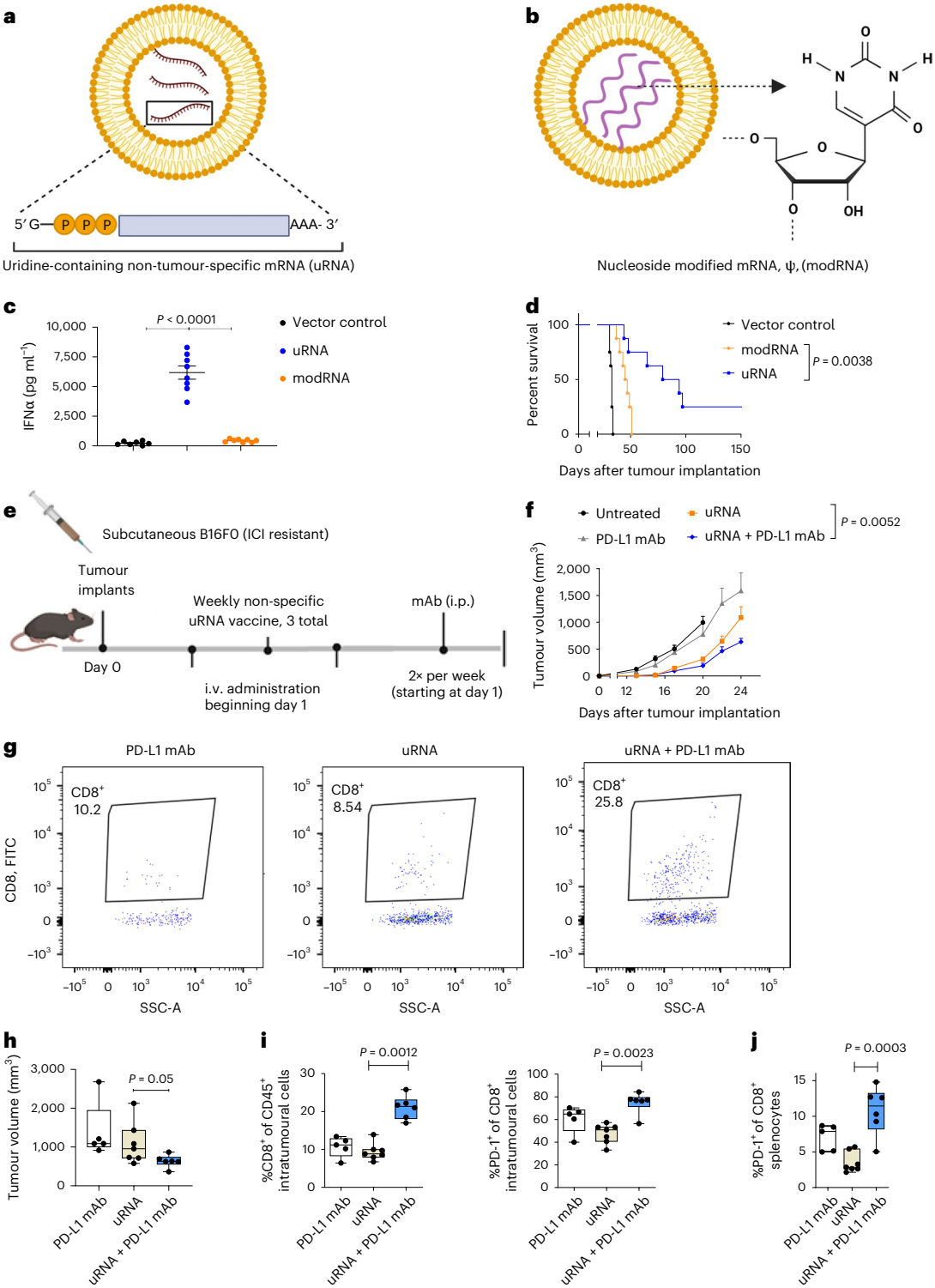

Fig. 4 | RNA encoding for non-tumour-specific IFN-I driver antigens (uRNA) sensitizes antigen recognition and ICI response. a,**b**, Diagram of liposomes loaded with uRNA (**a**) or nucleoside modRNA (**b**). **c**, C57Bl/6 mice ($n = 7–8$ per group) were vaccinated with OVA-encoding uRNA or modRNA versus vector control (empty LPs), and serum was collected from blood within 6 h for detection of IFNα levels by ELISA. **d**, C57Bl/6 mice bearing B16F10-OVA tumours ($n = 8$ per group) were vaccinated with OVA-encoding uRNA or modRNA once weekly ×3 vaccines. **e**, Treatment schema for **f**. **f**, C57Bl/6 mice ($n = 7–8$ per group) were subcutaneously inoculated with B16F0 tumours into the flank and vaccinated i.v. with luciferase-encoding uRNA on the following day with and without concomitant treatment with PD-L1 mAbs. **g**, Flow plots of intratumoural CD8 cells following each treatment condition. **h**, Boxplot of tumour volume measurements from **f** on day 24 (collection day) from remaining animals ($n = 5–7$ per group). **i**, Boxplot of intratumoural T cells by flow cytometry in B16F0 tumours from **f** on day 24 (collection day). **j**, Boxplot of splenocytes from **f** on day 24 (collection day) for PD-1$^+$ T cells by flow cytometry. Significance was determined via unpaired *t*-test (**c**), log-rank test (**d**), mixed-effect analysis/two-way ANOVA (**f**), Mann–Whitney test (**h**,**i**) and unpaired *t*-test (**j**). Boxplots display box at first and third quartile with line at median and whiskers from minimum to maximum datapoint values (**h**,**i**,**j**). Error bars are reported as s.e.m. (**c**,**f**). Panels **a**, **b** and **e** created with BioRender.com.

https://doi.org/10.1038/s41551-025-01380-1

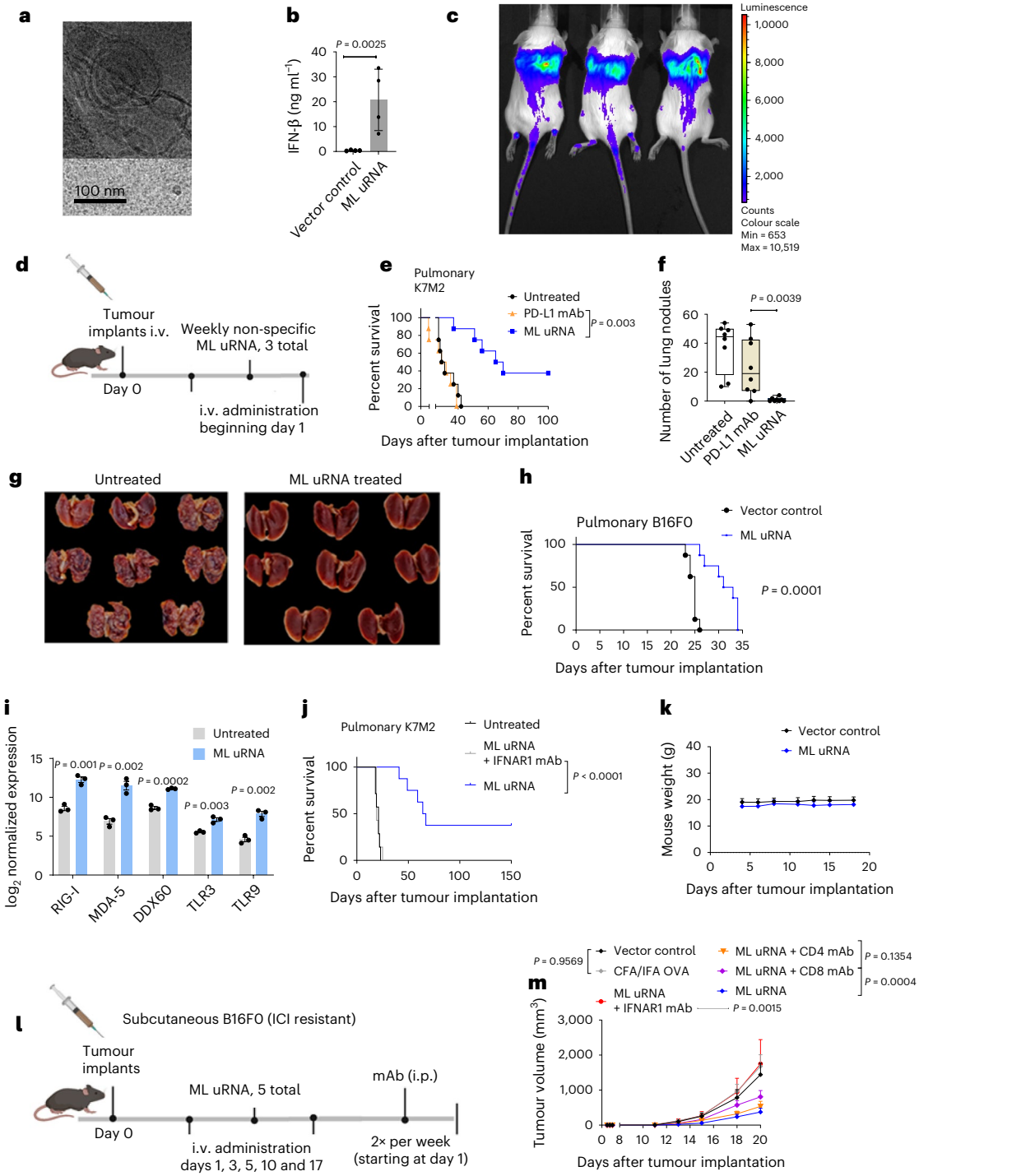

Fig. 5 | Monotherapy with ML uRNA induces anti-tumour efficacy. a, ML uRNA in LPAs by cryoelectron microscopy. Scale bar in electron micrograph superimposed on bottom of image to highlight region of interest. **b**, Serum measurements of IFN-I (IFNβ) within 6 h of i.v. ML uRNA administration to C57Bl/6 mice ($n = 5$ per group). **c**, Luciferase-encoding ML uRNA was administered to Balb/c mice and imaged 6 h later for bioluminescence by in vivo imaging system. **d**, Treatment schema of **e**, **h** and **j**. **e**, Kaplan–Meier survival curve of pulmonary K7M2 tumours treated with anti-PD-L1 mAb or i.v. with GFP-encoding ML uRNA administrations ($n = 8$ per group). **f**,**g**, Boxplot of tumour lung nodules collected from animals ($n = 8$ per group) bearing pulmonary K7M2 tumours treated with anti-PD-L1 mAb or GFP-encoding ML uRNA (**f**), with visualization of whole lungs from collected animals (**g**). **h**, Kaplan–Meier survival curve of C57Bl/6 mice ($n = 8$ per group) bearing pulmonary B16F0 tumours treated i.v. with GFP-encoding ML uRNA. **i**, Balb/c mice ($n = 3$ per group) bearing pulmonary B16F0 tumours were left untreated or vaccinated i.v. with serial ML uRNA encoding for pp65 on days 1, 5, 10 and 15 before lungs were collected for evaluation of gene signatures for pattern recognition receptors. **j**, Kaplan–Meier survival curve of Balb/c mice ($n = 7$–8 per group) bearing pulmonary K7M2 tumours treated i.v. with GFP-encoding ML uRNA or concomitant i.p. anti-IFNAR1 mAb. **k**, Weights of C57Bl/6 mice (6–7-week-old) bearing subcutaneous B16F0 ($n = 8$ per group), treated i.v. with serial ML uRNA infusions and measured over time. **l**, Treatment schema for **m**. **m**, Tumour volumes of wild-type mice ($n = 7$–8 per group) implanted with B16F0 melanomas, treated locally with CFA/IFA OVA peptide vaccines and compared to i.v. ML uRNA (pp65) with and without concomitant mAbs for IFNAR1, CD4 or CD8. Following initial dosing with CFA OVA, IFA OVA was administered in alternating muscle compartments during follow-up administrations. Significance was determined via unpaired *t*-test (**b**,**i**), log-rank test (**e**,**h**,**j**) and Mann–Whitney test (**f**). Boxplots display box at first and third quartile with line at median and whiskers from minimum to maximum datapoint values (**f**). Error bars are reported as s.e.m. (**b**,**i**,**m**) and s.d. (**k**). Panels **d** and **l** created with BioRender.com.

https://doi.org/10.1038/s41551-025-01380-1

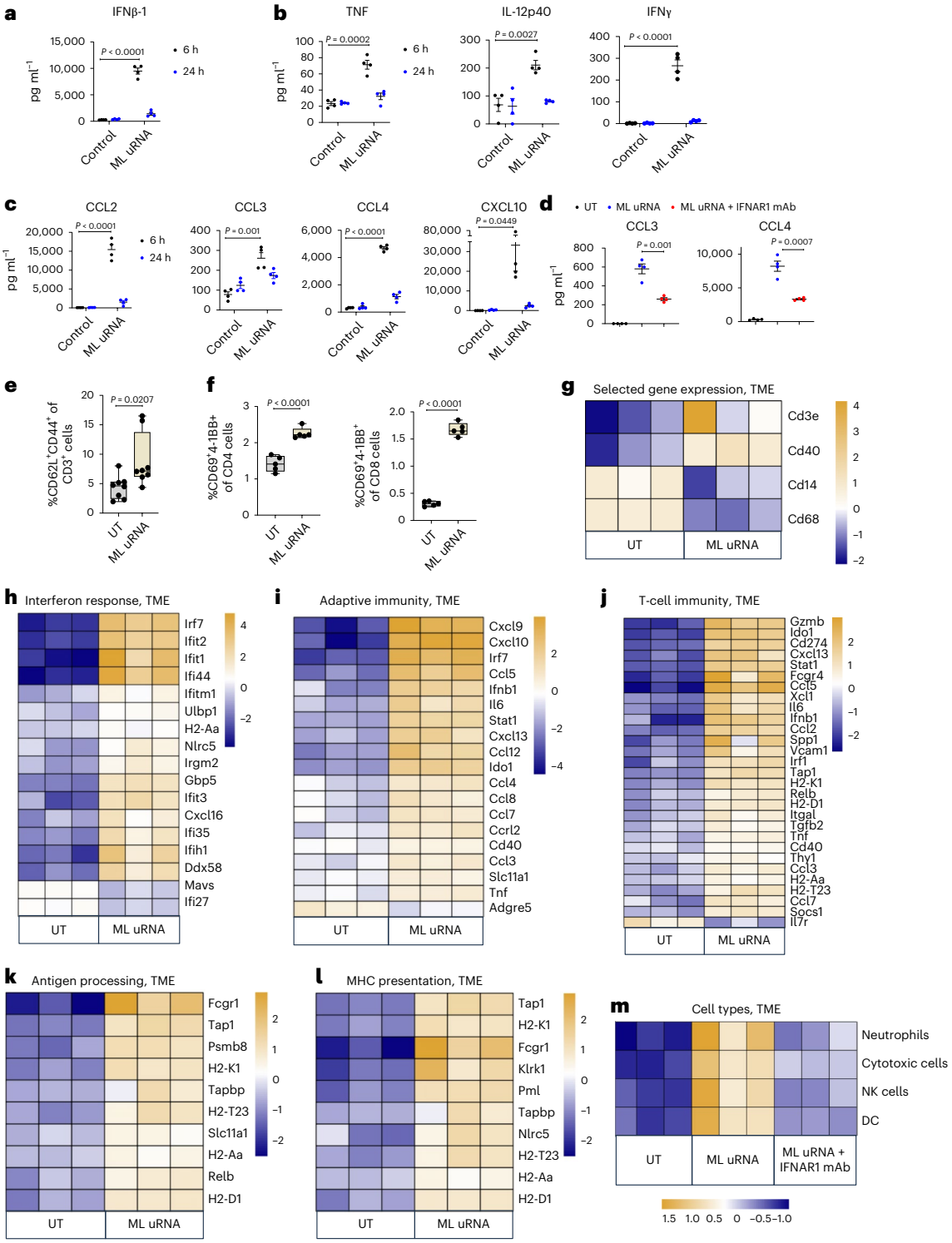

Fig. 6 | Serial administration of ML uRNA modulates the pulmonary TME in favour of effector immunity. a–**c**, Balb/c mice ($n = 4$ per group) bearing pulmonary K7M2 tumours had serum collected 6 h and 24 h after i.v. pp65 ML uRNA was administered on day 5. Serum was assessed for IFNβ (**a**), Th1 cytokines (**b**) and chemokines (**c**) by ELISA. **d**, ELISA of CCL3 and CCL4 6 h after i.v. ML uRNA with and without IFNAR1 mAbs. **e**, Boxplots of the percentage of intratumoural central memory T cells from Balb/c mice bearing pulmonary K7M2 ($n = 8$ per group) compared with untreated (UT) animals. Tumours were collected following 3 weekly i.v. ML uRNA (GFP). **f**, Boxplots of the percentage of $CD69^+$4-$1BB^+$ CD4 and $CD8^+$ splenocytes from C57Bl/6 mice ($n = 5$ per group) bearing B16F0 pulmonary tumours vaccinated i.v. with serial ML uRNA encoding for pp65 on days 1, 5, 10 and 15. **g**, Balb/c mice ($n = 3$ per group) bearing pulmonary K7M2 tumours received i.v. ML uRNA (pp65) on days 5, 7, 9, 16, 23 and 30 before tumour collection and gene expression analysis of CD3, CD40, CD14 and CD68. **h**–**m**, C57Bl/6 mice ($n = 3$ per group) bearing pulmonary B16F0 tumours received i.v. ML uRNA (pp65) on days 1, 5, 10 and 15 before tumour collection and nanostring analysis of interferon response (**h**), adaptive immunity (**i**), T-cell immunity (**j**), antigen processing (**k**), MHC presentation (**l**) and cell types (**m**), versus UT mice (**h**–**m**) and mice treated with concomitant IFNAR1 mAb (**m**). Significance was determined via unpaired *t*-test (**a**–**d**,**f**) and Mann–Whitney test (**e**). Boxplots display box at first and third quartile with line at median and whiskers from minimum to maximum datapoint values (**e**,**f**). Colour bars for heat maps represent distribution for $\log_2$ normalized expression (**g**–**l**) and cell types by *Z*-score (**m**). Error bars are reported as s.e.m. (**a**–**d**).

https://doi.org/10.1038/s41551-025-01380-1

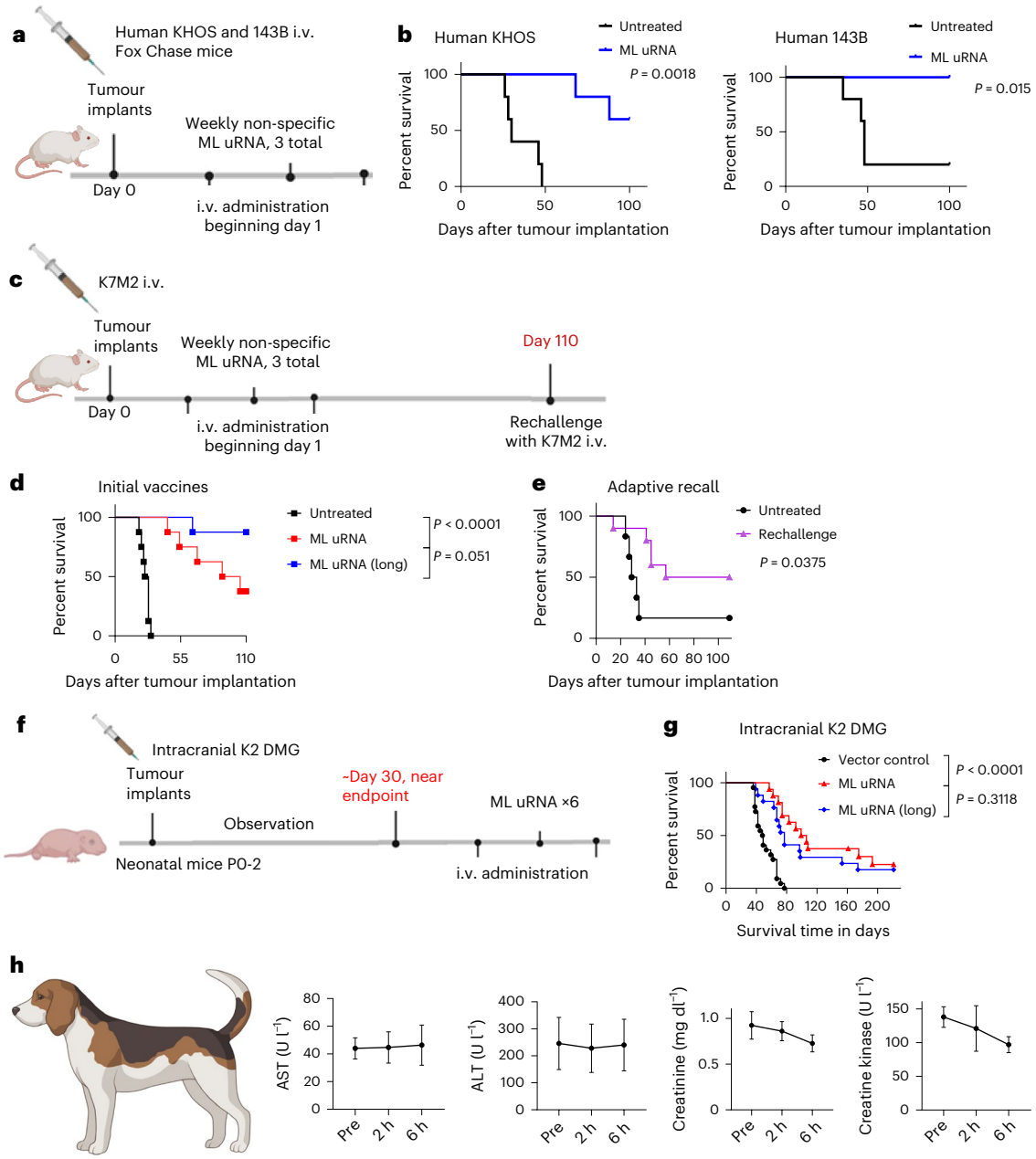

Fig. 7 | ML uRNA elicits activity against human cell line xenografts, confers protective recall responses and elicits long-term survival in animals near endpoint. a, Treatment schema of **b**. **b**, Kaplan–Meier survival curves of Fox Chase SCID mice ($n = 5$ per group) inoculated with KHOS or 143B human cell lines receiving i.v. ML uRNA (pp65) once weekly (×3). **c**, Treatment schema of **d** and **e**. Balb/c mice ($n = 8$ per group) bearing K7M2 tumours implanted i.v. on day 0 received i.v. ML uRNA encoding for GFP (ML uRNA) or pp65 (ML uRNA long) the following day and weekly thereafter (3 vaccines total). **d**, Survival curve of Balb/c mice ($n = 8$ per group) bearing pulmonary K7M2 tumours treated with GFP-encoding ML uRNA or pp65-encoding ML uRNA (long). **e**, Long-term survivors from **d** ($n = 10$) were challenged with K7M2 tumour cells and compared with age-matched untreated controls ($n = 5$). **f**, Treatment schema of **g**. **g**, K2 gliomas were implanted midline in neonatal C57Bl/6 pups at postnatal days 0–2. Mice were monitored for 4 weeks near endpoint before receiving vaccines. GFP-encoding ML uRNA or pp65-encoding ML uRNA (long) were administered intravenously at ~day 30; 3 administrations were administered in first week followed by once-weekly vaccines (×3). Kaplan–Meier curve displays the merge of 3 separate experiments for displayed groups ($n = 16$–21 per group). **h**, Canines ($n = 3$) with glioma diagnosis were treated i.v. with non-specific pp65 ML uRNA (single dose) after the owner's consent, and organ function tests for the liver (aspartate aminotransferase (AST)/alanine aminotransferase (ALT)), kidney (blood urea nitrogen, creatinine) and heart/muscle/brain (creatine kinase) were performed at pre, 2 h and 6 h after booster infusion. Significance was determined via log-rank test (**b**,**d**,**e**,**g**). Error bars are reported as s.e.m. (**h**). Panels **a**, **c**, **f** and **h** created with BioRender.com.

tumour implantation (Fig. 7f), ML uRNA encoding for either GFP or pp65 elicited significant anti-tumour efficacy (Fig. 7g). Unlike pulmonary tumours, there was no difference between longer uRNA length in intracranial tumour models, suggesting that differences between GFP and pp65 uRNAs may be due to localizing effects within the pulmonary TME. To ensure there was no acute toxicity, we performed end-organ toxicology within 24 h of ML uRNA which showed similar end-organ hematoxylin and eosin (H&E) findings between untreated and ML uRNA-treated animals (Supplementary Fig. 14 and Table 1). Since acute toxicities can occur over very short intervals and mice may not recapitulate the biological effects of large animals, we treated canines with non-specific ML uRNA (single dose) as previously described[24]

https://doi.org/10.1038/s41551-025-01380-1

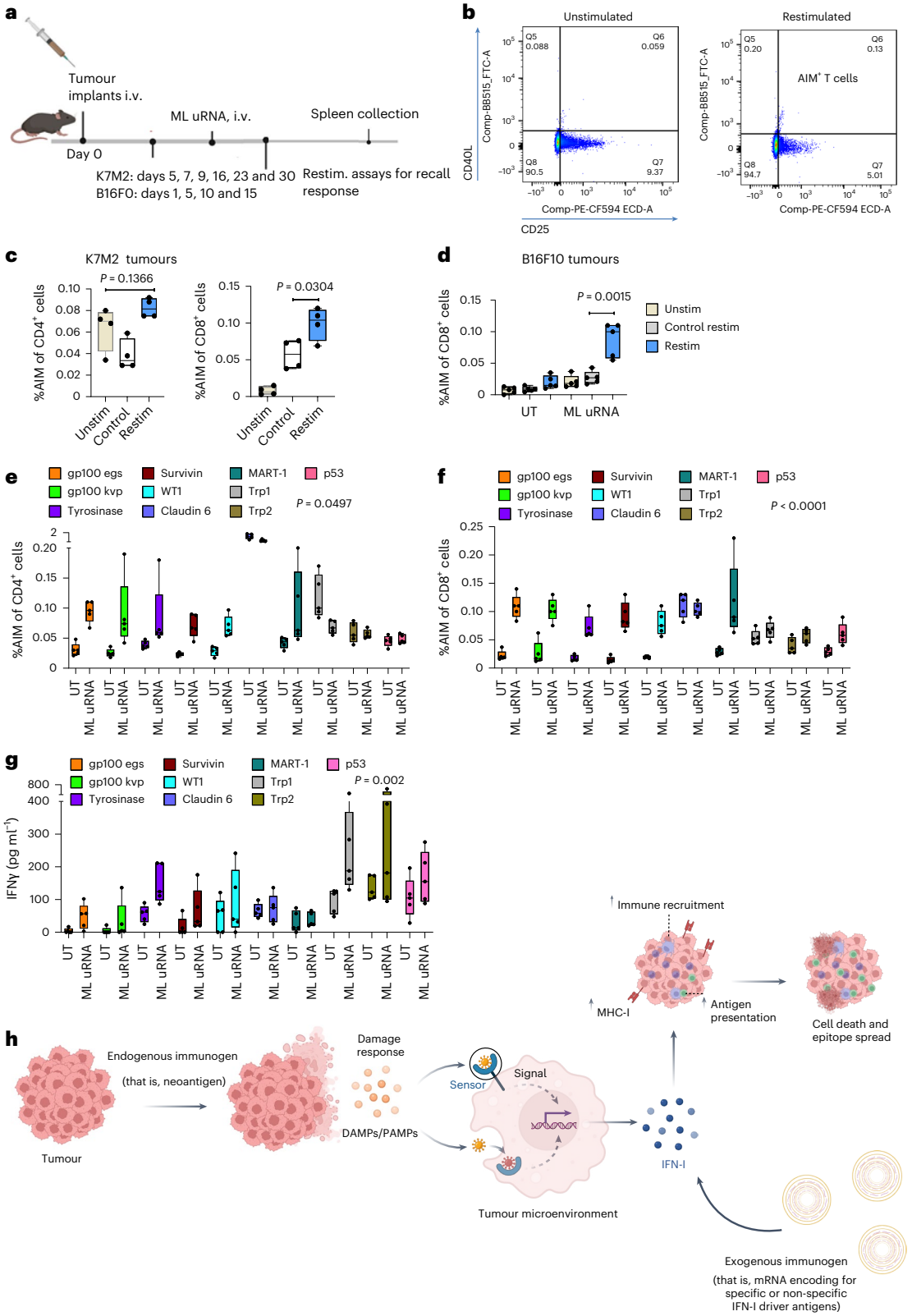

Fig. 8 | ML uRNA induces epitope spreading in poorly immunogenic murine models. a, Schema for restimulation assays including treatment regimen for K7M2 or B16F0 i.v. inoculated mice. **b**, Example of gating strategy for AIM assay. **c**,**d**, Mice bearing pulmonary K7M2 (**c**) ($n = 4$ per group) or B16F0 (**d**) ($n = 5$ per group) received i.v. ML uRNA (pp65) and spleens were collected for assessment of AIM$^+$ (CD40L$^+$CD25$^+$) CD4 and CD8 T cells. K7M2 and B16F0 restimulation was performed through co-culture of splenocytes with K7M2 or B16F0 cell lines, respectively, versus unstimulated splenocytes or control cell lines. **e**–**g**, Mice bearing pulmonary B16F0 ($n = 5$ per group) received i.v. ML uRNA (pp65), and spleens were collected for assessment of AIM$^+$ (CD40L$^+$CD25$^+$) CD4 (**e**) and CD8 (**f**) T cells after ex vivo restimulation with single overlapping peptides from 10 melanoma-associated antigens in the presence of IL-2. Supernatants were then collected for assessment of IFNγ recall responses (**g**). **h**, Illustration of tumour immunogenicity induced by neoantigens within TME or through exogenous RNA vaccination eliciting a damage response and epitope spreading. Significance was determined via unpaired *t*-test (**c**,**d**) and mixed-effect analysis/two-way ANOVA (**e**–**g**). DAMPs, damage-associated molecular patterns; PAMPs, pathogen-associated molecular patterns. Panels **a** and **h** created with BioRender.com.

and monitored acute changes in liver and kidney function tests, which remained stable 2–6 h post booster infusion (Fig. 7h).

While ML uRNA encoding for tumour-unspecific antigens can induce early IFN-I responses necessary for immunotherapeutic sensitization, we sought to determine direct evidence of epitope spreading against tumour-specific antigens in poorly immunogenic tumours (that is, K7M2 and B16F0). To more quantitatively assess epitope spreading, we leveraged an antigen-induced marker (AIM) assay that tags antigen-reactive T cells in response to tumour/peptide stimulus via double positive expression of T-cell activation markers (such as CD40L and CD25 co-expression), which can denote antigen-specific T cells in mice[26]. In animals vaccinated with ML uRNA, we demonstrate restimulation of AIM-reactive T cells following ex vivo co-culture with K7M2 tumour cells (Fig. 8a–c and Supplementary Fig. 15) and B16F0 in repeat studies (Fig. 8d). To demonstrate epitope spreading against melanoma-relevant antigens, we co-cultured isolated T cells from ML uRNA-treated mice with overlapping peptides from 10 tumour-associated antigens expressed in melanoma (including gp100 egs (EGSRNQDWL), gp100 kvp (KVPRNQDWL), tyrosinase, survivin, WTI, claudin 6, MART-1, Trp1, Trp2 and p53). In these co-culture assays, we found increases in AIM-reactive CD4 and CD8 T cells against nearly all selected peptides (Fig. 8e,f). These results were concordant with increases in IFNγ upon restimulation with each peptide (Fig. 8g), confirming epitope spreading in ML uRNA-treated animals. Overall, these data highlight that RNA biomimetics encoding for non-tumour-specific immunogens can incite a damage response that spills over to target more tumour-specific epitopes (Fig. 8h) resulting in long-term effectivity in poorly immunogenic tumour models. These observations may be used to universally vaccinate patients with immunologically 'cold' tumours.

Discussion

In recent years, our understanding of ICI response predictors has evolved, with several indicators such as PD-L1 expression[27], TMB[28] and microsatellite instability (MSI)[29] being proposed as potential determinants of therapeutic activity. However, these paradigms are confounded by the many patients with PD-L1-positive, MSI-high or TMB-high disease, who do not exhibit a favourable response to ICIs[30]. In addition, these conventional biomarkers do not address the intricate immunological cascade of events within the TME that underpins the effectiveness of ICI treatments. Therefore, a deeper understanding of these interactions is pivotal for identifying patients most likely to benefit from ICIs and for development of rational combination strategies to activate this cascade in ICI non-responsive patients.

Our understanding of cancer immunogenicity drivers remains limited. Studies have implicated the involvement of BATF3 expression, stimulator of interferon genes and interferon response factors in cancer immunogenicity[31–33]. The role of IFN-I in this context has been conflicting, with reports suggesting that it can exert both anti-tumoural and pro-tumoural effects[13,14,18,19]. Our study explored the impact of IFN-I signalling on cancer immunogenicity and response to ICIs. Early IFN-I responses are expected to be generated by both immune and non-immune cell types (stromal cells) in the TME, responding to the release of pathogen-associated molecular patterns and damage-associated molecular patterns from rapidly dividing and dying tumour cells releasing single-/double-stranded RNA/DNA that triggers various pattern recognition receptors (Toll-like receptors (TLRs), RIG-I-like receptors and cyclic GMP–AMP synthase–stimulator of interferon genes receptor activation). This is expected to happen naturally in ICI-responsive tumours but needs to be re-ignited in poorly immunogenic tumours.

We hypothesized that early IFN-I production (during tumourigenesis) is critical for initiating the cycle of cancer immunotherapy and could be exploited with RNA-encoding biomimetics. Early IFN-I signalling was critical in mediating ICI responsiveness in extracranial solid tumours and intracranial tumour models. In these models, IFN-I was more important than IFN-II (IFNγ) in eliciting a response to ICIs. While enrichment of type II IFN-responsive genes has been proposed as a predictive biomarker for ICI response[34], our data suggest that a fully coordinated immune response requires both innate (IFN-I) and adaptive (IFN-II) elements.

Notably, ICI response in sensitive tumours was transferable to resistant tumours in an IFN-I-dependent manner. In follow-up studies, we assessed whether ICI-resistant tumours could be sensitized through exogenous introduction or stimulation of IFN-I. We found that the intratumoural IFN-I was critical for inducing immunotherapeutic response and leveraged this understanding to create RNA biomimetics (uRNA) encoding for non-tumour-specific IFN-I driver antigens to depot within the TME. Non-tumour-specific RNA vaccines sensitized ICI response in poorly immunogenic murine models and could be used as a monotherapy to elicit IFN-I-dependent survivorship and epitope spreading in animals that warded off tumour rechallenge.

Although we have shown that late administration of uRNA can mediate anti-tumour efficacy, uRNA was administered early in many experiments. Early treatment may be used to clear micrometastatic disease and could be used in the future to replace 'preventative chemotherapy' which is probably harmful to an immunologic response. However, early-treatment models in small animals contain clinical relevancy concerns. To more appropriately model the clinical care scenario, investigating the protective effects of ML uRNA in murine resection models would be valuable follow-up studies.

Our findings suggest that the early presence of IFN-I signatures and its downstream effects in the TME might serve as a novel biomarker for predicting which patients have immunogenic tumours that are more likely to respond to ICIs. This knowledge could be used to identify PD-L1/TMB/MSI-low patients who may respond to ICIs through the presence of a single strong antigen that triggers an IFN-I response and epitope spreading. Although this phenomenon could conceivably occur in any malignancy and might explain anecdotal reports of ICI response in TMB-low tumours, TMB-high tumours are more likely to present strongly immunogenic or foreign epitopes. Identifying these driver antigens may be instrumental in distinguishing true immunotherapy responders from non-responders. In the absence of strong IFN-I driver antigens, we show that cancer immunogenicity can be sensitized through systemic administration of RNA-loaded biomimetics encoding for non-tumour-specific IFN-I driver antigens. These data could lead to the creation of a universal 'off the shelf' mRNA vaccine to sensitize cancer immunogenicity in prototypically 'cold' tumours. In summary, our findings challenge the prevailing notion that the limitations of immunotherapy are primarily dictated by the presence of a substantial mutational burden. Instead, our results indicate that successful cancer immunotherapy may be driven more by the presence of a strong, even irrelevant, antigenic stimulus initiating a damage response which can be restored by boosting early type-I interferon responses to enable epitope spreading and self-amplifying responses in treatment-refractory tumours.

Methods

Cell culture procedures

Tumour cell lines, B16F10-OVA and GL261, were procured as described in previous studies[20,24]. B16F0 and K7M2, murine melanoma and osteosarcoma cell lines, were purchased from ATCC (CRL-6322). B16F0 and B16F10-OVA were cultivated in DMEM medium supplemented with pyruvate, 10% fetal bovine serum (FBS) and 1% penicillin/streptomycin. Cells were maintained at 37 °C in a 5% CO_2 environment. Human KHOS and 143B osteosarcoma lines were purchased from ATCC. K2 glioma cells were provided as a kind gift from Dr Oren Becher as previously described[24]. Cell lines were authenticated on the basis of tumourigenicities of new cell line stocks and routinely tested and validated for contaminants including mycoplasma.

Tumour implantation protocols

Collection of B16F0, B16F10-OVA and GL261 cells from cultures involved treatment with 0.05% trypsin (Gibco), followed by washing in PBS containing serum and subsequent washing in PBS alone. Tumourigenic implantations were based on previously established methods for B16F10-OVA, GL261 B16F0, K7M2 and K2 (refs. 20,21,24,35). In experiments with human KHOS and 143B osteosarcoma lines, 1,250,000 cells were administered intravenously to each mouse. In experiments with incomplete tumourigenicities for B16F10-OVA, tumours were injected into either untreated naïve C57Bl/6 mice or mice pretreated with IFNAR1 mAb (500 µg, 24 h before and after tumour injections).

For subcutaneous implantation, subcutaneous injections of B16F0 and B16F10-OVA cells were administered into the right flank of anaesthetized C57Bl/6 mice using a 25-gauge syringe. Tumour dimensions were monitored three times weekly with a Westward digital caliper, and tumour volumes were calculated on the basis of measurements as previously described[20,21]. Intravenous injections of B16F0, K7M2 and B16F10-OVA cells were performed through i.v. tail vein injection to model pulmonary disease. Measurements were censored at early timepoints due to loss of animals in control groups with larger tumours and/or ulcerations that required humane killing at later timepoints.

For intracranial implantation, GL261 cells were resuspended in a PBS/methylcellulose mixture (1:1 ratio) before being stereotactically implanted intracranially (2 mm right of the bregma and 3 mm deep into the brain) with a Hamilton microlitre syringe (80000). K2 gliomas were injected into neonatal mice using methods previously described[24].

Mouse models

C57Bl/6, Balb/c and SCID (strain 001913), PMEL (strain 005023), IFNAR1 KO (strain 032045-JAX) and IFNγ (strain 002287) female/male mice of 5–7 weeks of age were acquired from Jackson Laboratories. Fox Chase mice were utilized for inoculation of human cell lines 143B and KHOS tumours. Animal experiments were conducted following protocols approved by the Institutional Animal Care and Use Committee (IACUC) at the University of Florida (protocol number 202009685). We complied with all relevant ethics regulations regarding animal care and use for experimental research. K7M2 tumours were injected into Balb/c mice and B16F0, GL261 and B16F10-OVA were implanted into C57Bl/6 mice. KHOS and 143B tumour cells were injected into Fox Chase mice. K2 tumours were implanted into neonatal C57Bl/6 mice at postnatal day 0–2. Following implantation, mice were blindly randomized, except for pre-implantation treatment groups. Luciferase imaging by in vivo imaging system was conducted as previously described[21]. Animal experiments were approved by the University of Florida IACUC for compliance with all relevant ethics guidelines.

Canine trial

Pet dogs diagnosed with glioma were enrolled through owner's consent in a University of Florida IACUC-approved trial administering tumour-unspecific RNA vaccine encoding for pp65 as previously described[24]. After single vaccine administration, serum chemistries were obtained for liver and renal function tests and creatine kinase levels. Serum chemistry was performed at UF College of Veterinary Medicine Small Animal Hospital. Animal experiments were approved by the University of Florida IACUC for compliance with all relevant ethics guidelines.

Antibodies

Checkpoint inhibition was achieved via the blockade of programmed cell death protein 1 or ligand-1 (PD-1 or PD-L1) signalling. Anti-PD-1 monoclonal antibody (mAb) (clone RMP1–14) and anti-PD-L1 mAb (clone 10F.9G2) were procured from Bio X cell and were delivered via i.p. injection to C57Bl/6 mice, using a 400-µg loading dose, followed by 200-µg dosing twice weekly. IFNAR1 blocking mAb (clone MAR1–5A3), CD4 mAb (clone GK1.5) and CD8α mAb (clone 2.43) were also sourced from Bio X cell and administered i.p. with a 500-µg, 200-µg and 200-µg loading dose, respectively, followed by respective maintenance doses of 250 µg, 100 µg and 100 µg twice weekly. For studies with RNA vaccines, mAb treatment was concurrent with vaccines.

IFNα administration

Recombinant mouse IFNα A protein (R&D Systems, 12100-1) was administered i.v. as a single dose on day 1 to the systemic treatment groups at a concentration of 10,000 IUs per mouse. For the IFNα cytokine culture groups, IFNα A was added to the cell culture medium 24 h before implantation. For the mixed treatment groups, it was included in the 1× PBS solution used to resuspend cells immediately before implantation. For tumour culture and IFNα intratumoural mixing, conditions were optimized to administer ~10,000 IUs of IFNα to each animal.

Peptide vaccines

Complete Freund's adjuvant (CFA; InvivoGen, vac-cfa-10) and OVA EndoFit (InvivoGen, vac-pova) were administered as a single/loading dose subcutaneously ~5 days post tumour implantation, following manufacturer protocol. Subsequent booster doses of incomplete Freund's adjuvant (IFA) mixed with OVA were administered subcutaneously on approximately days 7, 9, 16, 23 and 30, according to manufacturer guidelines. To prepare the emulsion, 50 µl of either CFA or IFA was mixed with 50 µl of 1 µg OVA dissolved in 1× PBS following manufacturer protocol, using a 21-gauge needle and syringe. The emulsion was mixed vigorously for several minutes to ensure stability and was vortexed before use.

RNA nanoliposomes and ML uRNA LPAs

Messenger RNA encoding for GFP and luciferase were packaged into nanoliposomes as previously described[20,21]. Briefly, full-length mRNAs were loaded and encapsulated into DOTAP liposomes generated through a thin-film rehydration method, followed by heating, sonication and extrusion. ML uRNA lipid particles were manufactured as LPAs and imaged via cryo-electron microscopy using previously described methods[24]. Briefly, upon addition of LP to uridine-containing mRNAs (15:1 mass ratio), multilamellar complexes were allowed to form and aggregates were injected intravenously without further disruption or extrusion.

RNA

RNAs were manufactured as previously described[24]. RNA encoding for GFP and luciferase was made in house and also purchased from Trilink Biotechnologies. pp65 mRNA was made as previously described[24]. uRNA references mRNA with naturally occurring unmodified uridines, and modRNA encoding for OVA was purchased from Trilink, with uridines modified using 5-methoxyuridine.

Enzyme-linked immunosorbent assays

Retro-orbital blood collection was carried out in C57Bl/6 mice, and serum was separated through coagulation and centrifugation processes. The detection of IFNα and IFNγ was conducted using an enzyme-linked immunosorbent assay (ELISA) kit (Thermo Fisher, BMS6027). Multiplex ELISA was performed through Eve Technologies using the Mouse Cytokine/Chemokine 44-Plex Discovery Biomarker Assay (MD44) following manufacturer preshipment preparation protocol.

Phagocyte depletion

For phagocyte depletion in vivo, clodronate liposomes procured from Liposoma were injected intravenously into the tail vein of C57Bl/6 mice using a loading dose of 200 µl. This phagocyte depletion protocol was initiated a day before intracranial tumour implantation.

Cell transfer assay

Mice were implanted with B16F10-OVA tumours (1,000,000 cells per animal) subcutaneously in the flank. Animals underwent treatment

with PD-1 mAb with and without IFNAR1 as described above. On day 21, splenocytes were collected and the CD3 fraction was purified using a Pan T-cell isolation kit before being adoptively transferred (~8 million cells per mouse) to new cohorts of animals inoculated with B16F0 (250,000 cells per animal) implanted into the flank.

Immunofluorescence staining

Mouse tissues were fixed in 4% paraformaldehyde overnight at 4 °C and submerged in 30% sucrose overnight at 4 °C. Post cryoprotection, tissues were embedded in OCT compound (Sakura, 4583), frozen at −80 °C, sectioned at ~30 µm using a Leica cryostat and placed on microscope slides, before storage at −20 °C. For immunostaining, sections were advanced to room temperature for 15 min and underwent three 5-min washes with PBS. Blocking solution was applied at room temperature for 1 h, containing 2% goat serum, 1% bovine serum albumin and 0.1% Triton X-100 in 1× PBS. After primary antibody incubation, sections were washed in PBS three times for 5 min each. Sections were subsequently stained with DAPI (1:3,000 in PBS) for 10 min at room temperature, washed with PBS three times for 5 min each and mounted with antifade mounting medium (Vector Laboratories, H-1700-10). Imaging was subsequently performed via a Leica Stellaris 8 WLL spectral confocal microscope. Image processing was conducted with a Fiji–ImageJ software (NIH).

In vitro cultures

B16F0 melanoma cells were seeded at a density of 100,000 cells per well in a 6-well plate. After 24 h, the cell count was expected to double to ~200,000 cells per well. Experiments were designed to include 3 wells per group that were cultured on separate plates. Each treatment well received either 375 µg of IFNAR1 mAb, 10,000 units of IFNα cytokine, or 300 µg of PD-1 mAb administered directly into the designated groups' culture medium 48 h before cell collection. The cell fraction was analysed for MHC-I and MHC-II expression using flow cytometry with standard Live/Dead APC-Cy7 staining protocol. For the P-mel co-culture experiments, B16F0 melanoma cells were seeded similarly at a density of 100,000 cells per well for expected doubling after 24 h. Splenocytes were collected from two pmel-1 mice (B6.Cg-Thy1a/Cy Tg(TcraTcrb)8Rest/J, Jackson Laboratories) using a 70-µm cell strainer, yielding a total of ~240 million cells. T-cell isolation was performed using a Pan T-cell Isolation Kit II (Miltenyi Biotec, 130-095-130) following manufacturer protocol, with a 1:10 ratio of T cells to B16F0 cells, and 2 million T cells were added per well. Cells were collected 48 h after the initiation of treatments for flow cytometric analysis.

3D culture

B16F0 melanoma and K7M2 tumour cells were suspended in an inert liquid-like solid solution and plated in a perfusion Darcy plate. A medical suction device was utilized to enable negative pressure that allowed media to gently perfuse via the interstitial spaces between liquid-like solid particles. This provided a continuous supply of nutrients to the cells and ensured the proper removal of metabolic waste. Cells formed tumour spheres. Spheres were treated with either IFNα cytokine alone or a combination of IFNα cytokine and IFNAR1 mAb. Immunofluorescent antibodies to detect MHC-I, PD-L1 and MHC-II expression were used on all groups, and an inverted microscope was used to take images for all previously mentioned channels.

Murine antigen recall assay

On harvest days for antigen recall assay experiments, mice were euthanized in a CO_2 chamber in compliance with humane practices and spleens were aseptically collected. Splenocytes were isolated via mechanical disruption and passed through a 70-µm filter (BD Biosciences, 352350). Following centrifugation, the cell pellet underwent lysis via BD Pharm Lyse lysing buffer (BD, 555899) and neutralized in complete T-cell medium composed of RPMI 1640 (Gibco, 11875-119), 10% FBS (Thermo Fisher, 35-011-CV), 1% penicillin/streptomycin (Gibco, 30-002-CI), 1% MEM non-essential amino acids (Gibco, 11140050), 1% sodium pyruvate (Gibco, 11360070) and 0.1% beta-mercaptoethanol (Gibco, 21985-023), all without added cytokines. T cells were purified using the Pan T-cell Isolation Kit II (Miltenyi Biotec, 130-095-130), enumerated and co-cultured at 500,000 cells per well with tumour cells or tumour-associated peptides in a 96-well round-bottom plate. The co-culture was maintained for 48 h in a 37 °C incubator supplemented with 5% CO_2. Co-culture was performed in the presence of human recombinant IL-2 (30 IU ml^{-1}) (from R&D). After co-culture, cells were collected for AIM assay using staining protocols to assess T-cell activation in response to the antigen recall.

In experiments with peptide restimulation for AIM assay, peptides were identified on the basis of their suggested upregulation in melanoma tumours[36–40] and co-cultures were performed as previously described[24]. Selected peptides including gp100 H2Db EGSRNQDWL, gp100 H2Db KVPRNQDWL, tyrosinase, survivin, WT1, claudin 6, MART-1, tyrosinase-related protein 1, tyrosinase-related protein 2 and p53 were prepared according to manufacturer instructions (JPT Peptide Technologies). Homology of human peptides with murine sequences was confirmed using NCBI BLAST to ensure a minimum of 70% similarity, thus verifying cross-species compatibility for immunogenicity studies.

Flow cytometry

Spleens and tumours from animals were collected and prepared into single-cell suspensions of white blood cells after RBC digestion. Cells were then stained as follows: CD8 FITC, PD-1 BV421, CD62L APC, CD44 PERCP5.5, Live/Dead APC-Cy7 and CD45 V500. Samples were run on FACS Canto/LSR flow cytometer. Gating of singlets from live cells was conducted on bulk populations. Intratumoural CD8 cells were gated on $CD45^+$ cells; peripheral cells ($PD\text{-}1^+$) from spleens were gated on CD8 cells. Intratumoural CD3 cells from a separate experiment were stained as follows: CD3 PE, CD62L APC, CD44 PERCP5.5, Live/Dead APC-Cy7. Multiparameter flow cytometry was leveraged to detect antigen-specific T cells using the AIM assay[26,41]. The surface markers utilized include CD3 (anti-mouse Alexa Fluor 700, Biolegend), CD4 (anti-mouse Pacific Blue, Biolegend), CD8 (anti-mouse APC-H7, BD), CD25 (anti-mouse PE/Dazzle 594, BD), CD69 (anti-mouse APC, Biolegend), 4-1BB (anti-mouse PE, Biolegend) and CD40L (anti-mouse FITC, Biolegend, 310804). Samples were run via a BD Symphony A3 flow cytometer and analysed using FlowJo 10.

RNA sequencing and analysis

A mouse tissue (50–100 mg) for each sample was acquired, QR coded and put in RNALater (AM7020, Thermo Fisher) for 24 h at 4 °C and long-term storage at −80 °C for batch isolation. To avoid noisy signals during analysis, necrotic cells were excluded, keeping the viability of bulk tumour cells. The specimens were homogenized by mechanical dissection and immediately transferred to TRIzol reagent (15596026, Invitrogen). Reagent volumes were adjusted on the basis of the tissues to optimize RNA yield and purity. To clean and purify RNA, we immediately used PureLink RNA mini kit (12183018A, Invitrogen).

RNA quality control and preparation. RNA isolated from samples were checked for quality and quantity using a Nanodrop One C spectrophotometer (Thermo Fisher). Samples deviating from the normal quality were checked using BioAnalyzer. All samples were also normalized to a uniform starting concentration on the basis of NanoString Technologies' established methods and protocols.

Gene expression profiling. NS_CancerImmune_V1.1 and XT Mm Glial Profiling CSO panels were used for gene expression profiling, comprising genes critical to immune response, oncogenesis and glial cell biology. The protocol hybridization times were modified to provide enough time for specific hybridization and avoid non-specific binding.

Normalization of gene expression data was achieved through the selective housekeeping genes for mouse tissue, by the geometric mean, using the nSolver Analysis Software to guarantee analytical consistency.

Differential expression analysis. The Rosalind platform was used to analyse differential gene expression variations in different biological pathways. Heat maps were made in R (v.4.2.2) using ggplot2 and pheatmap packages to show differential gene expression landscapes in all experimental cohorts.

Data and statistical analysis

The primary continuous outcome variables of interest, such as tumour volume and nodules, were obtained by calculating the mean and standard error for each group at timepoints along graphical illustrations. Tumour volume measurements were repeated measures from the same animal over time. Statistical analysis of tumour volumes was conducted using a mixed-effect analysis/two-way analysis of variance (ANOVA). When animals were lost following euthanasia during continuous timepoint measurements, mixed-effect analysis replaced two-way ANOVA in Prism statistical analysis. Comparisons for tumour and intratumoural analyses, such as for nodules/tumour volume and intratumoural T cells at discrete timepoints, were performed using the Mann–Whitney test, assuming the data were non-normally distributed. Immunologic parameters from the periphery comparing two independent groups were analysed using an unpaired *t*-test. The Kaplan–Meier method with a log-rank test was utilized for survival data. Data were validated across experiments in separate model systems. All statistical analyses were performed using Prism and were two-sided, and we considered $P < 0.05$ as the threshold for statistical significance. No adjustment for multiplicity was conducted in statistical inferences. Any additional materials, data and associated protocols could be made available upon reasonable request without undue qualifications. All efforts were made to be inclusive and objective in data reporting, with appropriate and ethical resource allocation.

Reporting summary

Further information on research design is available in the Nature Portfolio Reporting Summary linked to this article.

Data availability

The main data supporting the results in this study are available within the paper and its Supplementary Information and provided as supplementary source data. Raw data for sequencing results can be found at https://www.ncbi.nlm.nih.gov/geo/query/acc.cgi?acc=GSE255666. Source data are provided with this paper.

References

1. Bagchi, S., Yuan, R. & Engleman, E. G. Immune checkpoint inhibitors for the treatment of cancer: clinical impact and mechanisms of response and resistance. *Annu. Rev. Pathol.* **16**, 223–249 (2021).
2. Sharma, P. & Allison, J. P. The future of immune checkpoint therapy. *Science* **348**, 56–61 (2015).
3. Granier, C. et al. Mechanisms of action and rationale for the use of checkpoint inhibitors in cancer. *ESMO Open* **2**, e000213 (2017).
4. Wei, S. C., Duffy, C. R. & Allison, J. P. Fundamental mechanisms of immune checkpoint blockade therapy. *Cancer Discov.* **8**, 1069–1086 (2018).
5. Verma, V. et al. A systematic review of the cost and cost-effectiveness studies of immune checkpoint inhibitors. *J. Immunother. Cancer* **6**, 128 (2018).
6. Chauhan, A., Burkeen, G., Houranieh, J., Arnold, S. & Anthony, L. Immune checkpoint-associated cardiotoxicity: case report with systematic review of literature. *Ann. Oncol.* **28**, 2034–2038 (2017).
7. Snyder, A. et al. Genetic basis for clinical response to CTLA-4 blockade in melanoma. *N. Engl. J. Med.* **371**, 2189–2199 (2014).
8. Rizvi, N. A. et al. Mutational landscape determines sensitivity to PD-1 blockade in non-small cell lung cancer. *Science* https://doi.org/10.1126/science.aaa1348 (2015).
9. Kandoth, C. et al. Mutational landscape and significance across 12 major cancer types. *Nature* **502**, 333–339 (2013).
10. Fares, C. M., Van Allen, E. M., Drake, C. G., Allison, J. P. & Hu-Lieskovan, S. Mechanisms of resistance to immune checkpoint blockade: why does checkpoint inhibitor immunotherapy not work for all patients? *Am. Soc. Clin. Oncol. Educ. Book* **39**, 147–164 (2019).
11. Jenkins, R. W., Barbie, D. A. & Flaherty, K. T. Mechanisms of resistance to immune checkpoint inhibitors. *Br. J. Cancer* **118**, 9–16 (2018).
12. Morad, G., Helmink, B. A., Sharma, P. & Wargo, J. A. Hallmarks of response, resistance, and toxicity to immune checkpoint blockade. *Cell* **184**, 5309–5337 (2021).
13. Fuertes, M. B., Woo, S. R., Burnett, B., Fu, Y. X. & Gajewski, T. F. Type I interferon response and innate immune sensing of cancer. *Trends Immunol.* **34**, 67–73 (2013).
14. Benci, J. L. et al. Tumour interferon signaling regulates a multigenic resistance program to immune checkpoint blockade. *Cell* **167**, 1540–1554.e12 (2016).
15. Wang, X. et al. Suppression of type I IFN signaling in tumours mediates resistance to anti-PD-1 treatment that can be overcome by radiotherapy. *Cancer Res.* **77**, 839–850 (2017).
16. Jacquelot, N. et al. Sustained type I interferon signaling as a mechanism of resistance to PD-1 blockade. *Cell Res.* **29**, 846–861 (2019).
17. Zhou, L. et al. A dual role of type I interferons in antitumour immunity. *Adv. Biosyst.* **4**, e1900237 (2020).
18. Diamond, M. S. et al. Type I interferon is selectively required by dendritic cells for immune rejection of tumours. *J. Exp. Med.* **208**, 1989–2003 (2011).
19. Fuertes, M. B. et al. Host type I IFN signals are required for antitumour $CD8^+$ T cell responses through $CD8\alpha^+$ dendritic cells. *J. Exp. Med.* **208**, 2005–2016 (2011).
20. Sayour, E. J. et al. Personalized tumour RNA loaded lipid-nanoparticles prime the systemic and intratumoural milieu for response to cancer immunotherapy. *Nano Lett.* **18**, 6195–6206 (2018).
21. Sayour, E. J. et al. Systemic activation of antigen-presenting cells via RNA-loaded nanoparticles. *Oncoimmunology* **6**, e1256527 (2016).
22. Kariko, K., Buckstein, M., Ni, H. & Weissman, D. Suppression of RNA recognition by Toll-like receptors: the impact of nucleoside modification and the evolutionary origin of RNA. *Immunity* **23**, 165–175 (2005).
23. Baklaushev, V. P. et al. Luciferase expression allows bioluminescence imaging but imposes limitations on the orthotopic mouse (4T1) model of breast cancer. *Sci. Rep.* **7**, 7715 (2017).
24. Mendez-Gomez, H. R. et al. RNA aggregates harness the danger response for potent cancer immunotherapy. *Cell* **187**, 2521–2535.e1 (2024).
25. Ansari, A. M. et al. Cellular GFP toxicity and immunogenicity: potential confounders in in vivo cell tracking experiments. *Stem Cell Rev. Rep.* **12**, 553–559 (2016).
26. Poloni, C. et al. T-cell activation-induced marker assays in health and disease. *Immunol. Cell Biol.* **101**, 491–503 (2023).
27. Reck, M. et al. Updated analysis of KEYNOTE-024: pembrolizumab versus platinum-based chemotherapy for advanced non-small-cell lung cancer with PD-L1 tumour proportion score of 50% or greater. *J. Clin. Oncol.* **37**, 537–546 (2019).
28. Samstein, R. M. et al. Tumour mutational load predicts survival after immunotherapy across multiple cancer types. *Nat. Genet.* **51**, 202–206 (2019).

29. Llosa, N. J. et al. The vigorous immune microenvironment of microsatellite instable colon cancer is balanced by multiple counter-inhibitory checkpoints. *Cancer Discov.* **5**, 43–51 (2015).
30. Valero, C. et al. Response rates to anti-PD-1 immunotherapy in microsatellite-stable solid tumours with 10 or more mutations per megabase. *JAMA Oncol.* **7**, 739–743 (2021).
31. Hildner, K. et al. Batf3 deficiency reveals a critical role for CD8α$^+$ dendritic cells in cytotoxic T cell immunity. *Science* **322**, 1097–1100 (2008).
32. Woo, S. R. et al. STING-dependent cytosolic DNA sensing mediates innate immune recognition of immunogenic tumours. *Immunity* **41**, 830–842 (2014).
33. Suschak, J. J., Wang, S., Fitzgerald, K. A. & Lu, S. A cGAS-independent STING/IRF7 pathway mediates the immunogenicity of DNA vaccines. *J. Immunol.* **196**, 310–316 (2016).
34. Ayers, M. et al. IFN-γ-related mRNA profile predicts clinical response to PD-1 blockade. *J. Clin. Invest.* **127**, 2930–2940 (2017).
35. Karachi, A. et al. Modulation of temozolomide dose differentially affects T-cell response to immune checkpoint inhibition. *Neuro Oncol.* **21**, 730–741 (2019).
36. Zhai, Y. et al. Cloning and characterization of the genes encoding the murine homologues of the human melanoma antigens MART1 and gp100. *J. Immunother.* **20**, 15–25 (1997).
37. Zhang, C. et al. Identification of Claudin-6 as a molecular biomarker in pan-cancer through multiple omics integrative analysis. *Front. Cell Dev. Biol.* **9**, 726656 (2021).
38. Mansour, M. et al. Therapy of established B16-F10 melanoma tumours by a single vaccination of CTL/T helper peptides in VacciMax. *J. Transl. Med.* **5**, 20 (2007).
39. Rosenberg, S. A. Development of cancer immunotherapies based on identification of the genes encoding cancer regression antigens. *J. Natl Cancer Inst.* **88**, 1635–1644 (1996).
40. Overwijk, W. W. & Restifo, N. P. B16 as a mouse model for human melanoma. *Curr. Protoc. Immunol.* https://doi.org/10.1002/0471142735.im2001s39 (2001).
41. Balmas, E. et al. Islet-autoreactive CD4$^+$ T cells are linked with response to alefacept in type 1 diabetes. *JCI Insight* https://doi.org/10.1172/jci.insight.167881 (2023).

Acknowledgements

We thank G. Moore for assistance with veterinary animal experiments; D. Li and Biostatistics and Computational Biology Shared Resource for statistical support; L. Fagman and K. Young for help with large animals; and A. Dongtao Fu of the UF Molecular Pathology Core at the Department of Pathology, Immunology and Laboratory Medicine for assistance with genomics experiments. Cartoon images including those for mouse, canine, and schematics in figures were created with BioRender.com. This work was supported by federal awards W81XWH-17-1-0510, K08CA199224, R37CA251978, R01CA266857, R01FD007268 (FDA – OOPD, Office of Orphan Products Development), and P30CA247796; Florida Department of Health 20B11 (Bankhead Coley) and 20L07 (Live Like Bella) awards; and foundation grants from CureSearch (Catapult Award), Alex's Lemonade Stand (R Accelerated Award), Rally Foundation, Hyundai Hope on Wheels (Hope Scholar Award), Stop Children's Cancer and the Bonnie R. Freeman Professorship for Pediatric Oncology Research, Danny's Dream, the Medulloblastoma Initiative (MBI) and Cure Group 4 Medulloblastoma Consortium, Ians Friends Foundation, and the National Pediatric Cancer Foundation.

Author contributions

S.Q., B.W. and B.D.S. designed and performed the experiments, interpreted the data and co-wrote the paper. D.Z. conducted experimental studies and generated RNA vaccine reagents. J.M., F.W. and J.C.-R. conducted experiments. A.G. assisted with experiments and co-wrote the paper. A.D., C.Z., C.M., A.K., C.X., G.J., R.L., S.M., X.M., R.S.F.M., C.v.R., D.T.N., L.E., N.T., A.B., H.G., Y.C., E.O-R, C.R. and D.S. conducted/assisted with experiments. J.H. provided resources and oversight. S.C.-J. led canine studies. K.F. led H&E organ analyses. N.L.S., W.G.S., M.R., J.A.L. and C.T.F. provided critical resources and oversight. J.-H.L. oversaw statistical analyses. D.A.M. provided key resources and oversight. P.C. and H.R.M.-G. designed and performed experiments, interpreted data and co-wrote the paper. E.J.S. conceived and designed studies, performed experiments, provided resources and co-wrote the paper.

Competing interests

D.A.M. and C.T.F. hold an ownership interest in iOncologi, Inc. W.G.S. holds interest in Aurita, Inc. E.J.S. is a paid consultant for Siren Biotechnology and serves on the external advisory board of Nature's Toolbox with stock options. The paper discusses pending patent applications from S.Q., J.M., A.G., W.G.S., M.R., D.A.M., P.C., H.R.M.-G. and E.J.S, some of which are licensed to iOncologi, Inc. H.R.M.-G. and E.J.S. receive royalty payments from iOncologi, Inc.

Additional information

Supplementary information The online version contains supplementary material available at https://doi.org/10.1038/s41551-025-01380-1.

Correspondence and requests for materials should be addressed to Elias J. Sayour.

Peer review information *Nature Biomedical Engineering* thanks Yang-Xin Fu and the other, anonymous, reviewer(s) for their contribution to the peer review of this work.

Reprints and permissions information is available at www.nature.com/reprints.

Publisher's note Springer Nature remains neutral with regard to jurisdictional claims in published maps and institutional affiliations.

[1]Lillian S. Wells Department of Neurosurgery, Preston A. Wells, Jr. Center for Brain Tumor Therapy, McKnight Brain Institute, University of Florida, Gainesville, FL, USA. [2]University of Florida Genetics Institute, University of Florida, Gainesville, FL, USA. [3]Department of Pediatrics, Division of Pediatric Hematology-Oncology, UF Health Cancer Center, University of Florida, Gainesville, FL, USA. [4]Department of Radiation Oncology, The University of Texas MD Anderson Cancer Center, Houston, TX, USA. [5]Department of Mechanical and Aerospace Engineering, University of Florida, Gainesville, FL, USA. [6]Department of Medicine, Division of Hematology and Oncology, UF Health Cancer Center, University of Florida, Gainesville, FL, USA. [7]College of Veterinary Medicine, University of Florida, Gainesville, FL, USA. [8]Department of Pathology, University of Florida, Gainesville, FL, USA. [9]Center of Immunotherapy and Precision Immuno-Oncology/Head and Neck Institute, Cleveland Clinic, Cleveland, OH, USA. [10]Department of Biostatistics, University of Florida, Gainesville, FL, USA. [11]These authors contributed equally: Sadeem Qdaisat, Brandon Wummer, Brian D. Stover. ✉e-mail: Elias.Sayour@neurosurgery.ufl.edu

nature portfolio

Corresponding author(s): Elias Sayour, MD,PhD

Last updated by author(s): 2024-August 25

Reporting Summary

Nature Portfolio wishes to improve the reproducibility of the work that we publish. This form provides structure for consistency and transparency in reporting. For further information on Nature Portfolio policies, see our Editorial Policies and the Editorial Policy Checklist.

Statistics

For all statistical analyses, confirm that the following items are present in the figure legend, table legend, main text, or Methods section.

n/a	Confirmed
☐	☒ The exact sample size (*n*) for each experimental group/condition, given as a discrete number and unit of measurement
☐	☒ A statement on whether measurements were taken from distinct samples or whether the same sample was measured repeatedly
☐	☒ The statistical test(s) used AND whether they are one- or two-sided *Only common tests should be described solely by name; describe more complex techniques in the Methods section.*
☒	☐ A description of all covariates tested
☐	☒ A description of any assumptions or corrections, such as tests of normality and adjustment for multiple comparisons
☐	☒ A full description of the statistical parameters including central tendency (e.g. means) or other basic estimates (e.g. regression coefficient) AND variation (e.g. standard deviation) or associated estimates of uncertainty (e.g. confidence intervals)
☐	☒ For null hypothesis testing, the test statistic (e.g. *F*, *t*, *r*) with confidence intervals, effect sizes, degrees of freedom and *P* value noted *Give P values as exact values whenever suitable.*
☒	☐ For Bayesian analysis, information on the choice of priors and Markov chain Monte Carlo settings
☒	☐ For hierarchical and complex designs, identification of the appropriate level for tests and full reporting of outcomes
☒	☐ Estimates of effect sizes (e.g. Cohen's *d*, Pearson's *r*), indicating how they were calculated

Our web collection on statistics for biologists contains articles on many of the points above.

Software and code

Policy information about availability of computer code

Data collection	No original code was used for scientific results and conclusions. Data was collected using Microsoft Office programs
Data analysis	Data was analyzed using GraphPad Prism (Version 10), Microsoft Excel (Microsoft 365 products), Rosalind, and FlowJo (Version 10) software.

For manuscripts utilizing custom algorithms or software that are central to the research but not yet described in published literature, software must be made available to editors and reviewers. We strongly encourage code deposition in a community repository (e.g. GitHub). See the Nature Portfolio guidelines for submitting code & software for further information.

Data

Policy information about availability of data

All manuscripts must include a data availability statement. This statement should provide the following information, where applicable:

- Accession codes, unique identifiers, or web links for publicly available datasets
- A description of any restrictions on data availability
- For clinical datasets or third party data, please ensure that the statement adheres to our policy

The main data supporting the results in this study are available within the paper and its Supplementary Information and provided as supplementary Source Data. Raw data for sequencing results can be found at https://www.ncbi.nlm.nih.gov/geo/query/acc.cgi?acc=GSE255666.

Research involving human participants, their data, or biological material

Policy information about studies with human participants or human data. See also policy information about sex, gender (identity/presentation), and sexual orientation and race, ethnicity and racism.

Reporting on sex and gender	This study did not involve human subjects
Reporting on race, ethnicity, or other socially relevant groupings	This study did not involve human subjects
Population characteristics	This study did not involve human subjects
Recruitment	This study did not involve human subjects
Ethics oversight	This study did not involve human subjects

Note that full information on the approval of the study protocol must also be provided in the manuscript.

Field-specific reporting

Please select the one below that is the best fit for your research. If you are not sure, read the appropriate sections before making your selection.

☒ Life sciences ☐ Behavioural & social sciences ☐ Ecological, evolutionary & environmental sciences

For a reference copy of the document with all sections, see nature.com/documents/nr-reporting-summary-flat.pdf

Life sciences study design

All studies must disclose on these points even when the disclosure is negative.

Sample size	Effect sizes were not predetermined. Details regarding sample size, technical/biological replicates are included in figure legends.
Data exclusions	Data exclusions are mentioned in manuscript and pertain to animals requiring pre-established euthanasia prior to termination of the experimental studies.
Replication	Observations were repeated across experiments and experimental repeats
Randomization	When possible, animals were randomized before treatment
Blinding	When possible, investigators were blinded during treatment administrations and data collection

Reporting for specific materials, systems and methods

We require information from authors about some types of materials, experimental systems and methods used in many studies. Here, indicate whether each material, system or method listed is relevant to your study. If you are not sure if a list item applies to your research, read the appropriate section before selecting a response.

Materials & experimental systems

n/a	Involved in the study
☐	☒ Antibodies
☐	☒ Eukaryotic cell lines
☒	☐ Palaeontology and archaeology
☐	☒ Animals and other organisms
☒	☐ Clinical data
☒	☐ Dual use research of concern
☒	☐ Plants

Methods

n/a	Involved in the study
☒	☐ ChIP-seq
☐	☒ Flow cytometry
☒	☐ MRI-based neuroimaging

Antibodies

Antibodies used	Antibodies for in vivo use: Anti-PD-1 monoclonal antibody (mAb) (clone: RMP1−14), Bioxcell Anti-PD-L1 mAb (clone: 10F.9G2TM), Bioxcell

IFNAR1 blocking mAb (clone: MAR1–5A3), Bioxcell
CD4 mAb (Clone: GK1.5), Bioxcell
CD8α mAb (Clone: 2.43), Bioxcell

Validation

Depleting and blocking antibodies have been validated in efficacy studies in tumor bearing mice; Flow antibodies have been validated by manufacturer

Eukaryotic cell lines

Policy information about cell lines and Sex and Gender in Research

Cell line source(s)	Sources of cell lines disclosed in methods. B16F10-OVA were received as a kind gift from Richard Vile (Mayo Clinic). K2 glioma cells were received as a kind gift from Oren Becher (Northwestern University). GL261 cells were received as a kind gift from John Sampson (Duke University) and from the DCTD Tumor Repository at the NCI. 143B, KHOS, K7M2 and B16F0 were purchased from ATCC.
Authentication	Cell lines are authenticated by commercial vendor (e.g. ATCC), gross pathology and/or H&E staining from in vivo studies
Mycoplasma contamination	Our cell lines are routinely tested for contaminants
Commonly misidentified lines (See ICLAC register)	Misidentified cells were not used in the study

Animals and other research organisms

Policy information about studies involving animals; ARRIVE guidelines recommended for reporting animal research, and Sex and Gender in Research

Laboratory animals	C57Bl/6, Balb/c, and SCID (Strain: 001913), PMEL (Strain: 005023), IFNAR1 KO (Strain: 032045-JAX), IFN-γ (Strain: 002287) mice of 5-7 weeks of age were acquired from Jackson Laboratories. Fox Chase mice were utilized for inoculation of human cell lines
Wild animals	This study did not use wild animals but involved pet dogs enrolled onto a IACUC approved trial following owner's consent
Reporting on sex	Reported in Methods
Field-collected samples	Samples were not collected in the field
Ethics oversight	Research complies with ethical guidelines and was approved by the University of Florida institutional Animal Care and Use Committee

Note that full information on the approval of the study protocol must also be provided in the manuscript.

Plants

Seed stocks	This study did not involve plants
Novel plant genotypes	This study did not involve plants
Authentication	This study did not involve plants

Flow Cytometry

Plots

Confirm that:

☒ The axis labels state the marker and fluorochrome used (e.g. CD4-FITC).

☒ The axis scales are clearly visible. Include numbers along axes only for bottom left plot of group (a 'group' is an analysis of identical markers).

☒ All plots are contour plots with outliers or pseudocolor plots.

☒ A numerical value for number of cells or percentage (with statistics) is provided.

Methodology

Sample preparation	White blood cells were isolated via mechanical disruption and passed through a 70 µm filter (BD Biosciences, cat. 352350). Following centrifugation, the cell pellet was lysed using BD Pharm Lyse™ Lysing Buffer (BD, cat. 555899) and neutralized in complete T cell medium
Instrument	BD Symphony A3
Software	FlowJo 10
Cell population abundance	No FACsorting of rare populations performed
Gating strategy	Gating strategies provided in supplemental data

☒ Tick this box to confirm that a figure exemplifying the gating strategy is provided in the Supplementary Information.